**Atmospheric
Chemistry
and Physics
Discussions**

ACPD

5, 4545–4597, 2005

Earth's surface
shortwave radiation
budget

N. Hatzianastassiou et al.

Title Page

Abstract	Introduction
Conclusions	References
Tables	Figures

Global distribution of Earth's surface shortwave radiation budget

N. Hatzianastassiou[1,2]**, C. Matsoukas**[2,3]**, A. Fotiadi**[2]**, K. G. Pavlakis**[2,5]**,
E. Drakakis**[2,4]**, D. Hatzidimitriou**[2,3]**, and I. Vardavas**[2,3]

[1]Laboratory of Meteorology, Department of Physics, University of Ioannina, Greece
[2]Foundation for Research and Technology-Hellas, Heraklion, Crete, Greece
[3]Department of Physics, University of Crete, Crete, Greece
[4]Department of Electrical Engineering, Technological Educational Institute of Crete, Greece
[5]Department of General Applied Science, Technological Educational Institute of Crete, Greece

EGU

N. Hatzianastassiou et al.

Full Screen / Esc

Print Version

Interactive Discussion

EGU

Abstract

The monthly mean shortwave (SW) radiation budget at the Earth's surface (SRB) was computed on 2.5-degree longitude-latitude resolution for the 17-year period from 1984 to 2000, using a radiative transfer model accounting for the key physical parameters that determine the surface SRB, and long-term climatological data from the International Satellite Cloud Climatology Project (ISCCP-D2). The model input data were supplemented by data from the National Centers for Environmental Prediction – National Center for Atmospheric Research (NCEP-NCAR) and European Center for Medium Range Weather Forecasts (ECMWF) Global Reanalysis projects, and other global data bases such as TIROS Operational Vertical Sounder (TOVS) and Global Aerosol Data Set (GADS). The model surface radiative fluxes were validated against surface measurements from 22 stations of the Baseline Surface Radiation Network (BSRN) covering the years 1992–2000, and from 700 stations of the Global Energy Balance Archive (GEBA), covering the period 1984–2000. The model is in very good agreement with BSRN and GEBA, with a negative bias of 14 and 6.5 Wm^{-2}, respectively. The model is able to reproduce interesting features of the seasonal and geographical variation of the surface SW fluxes at global scale, which is not possible with surface measurements. Based on the 17-year average model results, the global mean SW downward surface radiation (DSR) is equal to 171.6 Wm^{-2}, whereas the net downward (or absorbed) surface SW radiation is equal to 149.4 Wm^{-2}, values that correspond to 50.2 and 43.7% of the incoming SW radiation at the top of the Earth's atmosphere. These values involve a long-term surface albedo equal to 12.9%. Significant increasing trends in DSR and net DSR fluxes were found, equal to 4.1 and 3.7 Wm^{-2}, respectively, over the 1984–2000 period (equivalent to 2.4 and 2.2 Wm^{-2} per decade), indicating an increasing surface solar radiative heating. This surface SW radiative heating is primarily attributed to clouds, especially low-level, and secondarily to other parameters such as total precipitable water. The surface solar heating occurs mainly in the period starting from the early 1990s, in contrast to the commonly reported decreasing trend in DSR

Earth's surface shortwave radiation budget

N. Hatzianastassiou et al.

through the late 1980s, found also in our study. The computed global mean DSR and net DSR flux anomalies were found to range within ± 8 and $\pm 6\,\mathrm{Wm}^{-2}$, respectively, with signals from El Niño and La Niña events, and the Pinatubo eruption, whereas significant positive anomalies have occurred in the period 1992–2000.

1. Introduction

Knowledge and monitoring of the Earth's radiation budget (ERB) is essential for improving our understanding of the Earth's climate and potential climatic changes (IPCC, 2001), since the radiative energy exchanges at the top of the atmosphere (TOA) and at the Earth's surface regulate the redistribution of energy and determine the energy balance of the Earth-atmosphere system. Rather than examining ERB as a whole, it is very important to quantify its components, namely the Earth's radiation budget at TOA (TOARB), within the atmosphere, and at the surface (SRB). Attempts to construct a global annual mean ERB date back to the beginning of the 20th century (Abbot and Fowle, 1908; Dines et al., 1917). Meanwhile, there has been a long history of other early studies (e.g. Houghton, 1954; Budyko, 1956; London, 1957), but all these studies were severely limited by the lack of knowledge of planetary albedo. Satellite observations, such as those from Nimbus-7 and the Earth Radiation Budget Experiment (ERBE) have greatly improved our knowledge of TOARB. Nevertheless, satellites do not measure directly radiative fluxes at the Earth's surface. Therefore, at present time, knowledge of SRB is far less advanced than the one for TOARB. The SRB, however, is a major component of the energy exchanges between the atmosphere and the land/ocean surface, and hence affects temperature fields, atmospheric and oceanic circulation, and the hydrological cycle. For example, about half of the solar energy absorbed at the surface is used to evaporate water, which eventually forms clouds (Li et al., 1997). Besides, SRB data constitute a valuable resource for initialising and testing climate and general circulation models (GCMs). The estimation of SRB represents one of the most significant objectives of the World Climate Research Programme (WCRP)

as demonstrated by its Global Energy and Water Cycle Experiment (GEWEX), and in particular the GEWEX SRB project (Stackhouse et al., 1999; Gupta et al., 1999).

Due to the inability of directly measuring radiation at the Earth's surface with satellites, the SRB has to be derived. On the other hand, surface observations cannot solve the problem, because of the sparsity and nonhomogeneity of stations (Li and Leighton, 1993; Li et al., 1997), especially over oceans. Thus, global atlases from surface-based observations (Esbensen and Kushnir, 1981) suffer from this shortcoming. Therefore, the modelling approach remains as the only alternative, provided that the model results can be trusted through validation against quality measurements. One way to solve the problem is to establish correlations between TOA and surface radiative fluxes in order to derive surface fluxes directly using the satellite measurements of TOA fluxes (Ramanathan, 1986; Schmetz, 1989; Weare, 1989; Cess et al., 1991; Darnell et al., 1992; Pinker and Laszlo, 1992; Li and Leighton, 1993). Although this technique was initially shown to work quite properly for SRB (Cess et al., 1991; Li et al., 1993), a strong debate was initiated by studies claiming that there is a substantial underestimation of solar absorption by clouds (Cess et al., 1995; Ramanathan et al, 1995; Pilewski and Valero, 1995), while other studies have challenged this (Chou et al., 1995; Li et al., 1995; Arking et al., 1996). Thus, there is a serious uncertainty regarding the reliability of the correlations for producing surface SW fluxes (Gupta et al., 1999). Another way to solve the problem of estimating SRB is to develop algorithms and models to compute SRB fluxes on a global scale using observations of atmospheric, cloud, and surface properties, preferably from operational satellite sources to provide global coverage. Following the early work of London (1957), a series of modelling studies (Manabe and Strickler, 1964; Vonder Haar and Suomi, 1971; Sasamori et al., 1972; Raschke et al., 1973; Ellis and Vonder Haar, 1976; Jacobowitz et al., 1979; Gautier et al., 1980; Stephens et al., 1981; Budyko, 1982) made use of satellite data available at that time. Since then, the amount and quality of satellite data have substantially improved, especially in terms of clouds (whose some properties, such as cloud optical depth, represented the most difficult parameters to be derived for many years) with the International Satellite

**Earth's surface
shortwave radiation
budget**

N. Hatzianastassiou et al.

EGU

Cloud Climatology Project (ISCCP, Rossow and Schiffer, 1991) that provides the most complete and comprehensive existing global cloud climatology. Thus, in the last two decades, a large number of studies estimating SRB have been published (e.g. Raschke et al., 1987; Darnell et al., 1988; Rossow and Lacis, 1990; Kyle at al., 1990; Stephens
5 and Greenwald, 1991; Darnell et al., 1992; Hartmann, 1993; Li and Leighton, 1993; Kiehl et al., 1995; Rossow and Zhang, 1995; Whitlock et al., 1995; Fowler and Randall, 1996; Del Genio et al., 1996; Chen and Roeckner, 1996; Wild et al., 1998a, b; Yu et al., 1999). Gupta et al. (1999) derived an 8-year (July 1983–June 1991) climatology of SRB by using satellite data from the ISCCP C-series, on a monthly mean basis.
10 Hatzianastassiou and Vardavas (1999, 2001) provided also an 8-year climatology of the SW radiation budget of the northern and southern hemispheres, respectively, but this was done only on a 10-degree latitude zonal and monthly mean basis. Furthermore, these studies have been performed by using data from the ISCCP-C2 series. The new ISCCP D-series data include significant improvements, especially in terms
15 of cloud structure and cloud detection over highly reflecting surfaces (cf. Rossow and Schiffer, 1999) and cover a longer time period, extending up to year 2000. This is important, since the Earth's radiation budget changes with time. Although the more recent energy budget studies, including those from GCMs, but also results from re-analysis projects (such as the National Centers for Environmental Prediction/National
20 Center for Atmospheric Research, NCEP/NCAR, or the European Center for Medium Range Weather Forecast, ECMWF), show good agreement with observations at TOA, there is a considerable variation for SW SRB (called henceforth simply SRB) within about $20 \, \mathrm{Wm}^{-2}$ (Kiehl and Trenberth, 1997). Moreover, estimated surface SW flux values tend to be systematically higher than ground-based station observations by sig-
25 nificant amounts (Garratt, 1994; Wild et al., 1995, 1998a, b; Li et al., 1997; Kiehl and Trenberth, 1997; Garratt et al., 1998). For example, the global and annual mean SW flux absorbed at the surface is generally larger than $170 \, \mathrm{Wm}^{-2}$, with the exception of the European Center/ Hamburg (ECHAM) model, while the only direct radiative surface flux measurements from the Global Energy Balance Archive (GEBA, Ohmura and

Earth's surface shortwave radiation budget

N. Hatzianastassiou et al.

Gilgen, 1993), which constitutes the "best" estimate of the globally averaged net SW flux, indicates values that are lower by about 20–25 Wm^{-2}.

In this study we provide a 17-year (January 1984–December 2000) climatology of the Earth's SRB, on a 2.5-degree longitude-latitude resolution, and on monthly mean basis. A physical deterministic radiative transfer model is used to compute the SRB components, i.e. the SW downward surface radiation (DSR) and the net downward (or absorbed) SW radiation (called henceforth net DSR) at the Earth's surface. More specifically, the seasonal and geographical variation of SRB components is investigated, whereas emphasis is given to patterns of averaged values over space and time, specific local and temporal characteristics, and inter-annual variability. The model computes the SW radiative fluxes in the atmosphere and the SW radiation budget at TOA and is described in detail by Hatzianastassiou et al. (2004a). Climatological data for the surface and atmospheric parameters which are relevant to the transfer of SW radiation, were taken from existing complete global data sets. Data for clouds, but also for other surface and atmospheric parameters were taken from ISCCP-D2, supplemented by humidity and temperature data taken from NCEP/NCAR and ECMWF reanalysis projects. Model input data were also taken from other global data bases, such as the Television Infrared Observational Satellite (TIROS) Operational Vertical Sounder (TOVS), whereas aerosol particles were accounted for in the study, by using relevant data from the Global Aerosol Data Set (GADS), as explained in Sect. 3. The model computations are validated at the pixel level against quality data from the Baseline Surface Radiation Network (BSRN) and GEBA. A brief description of the model is given in the next section, while Sect. 3 describes the model input data. The model results are given in Sect. 4, where patterns of seasonal and temporal distributions of SRB components are discussed on the basis of pixel-level model results, while mean hemispherical and global, along with mean annual SRB results are given and inter-annual variations and trends are examined. Section 5 provides a sensitivity analysis of SRB components to the various key surface and atmospheric parameters. The results of the model validation at pixel level against BSRN and GEBA stations are given in Sect. 6,

EGU

before the summary and conclusions (Sect. 7).

2. Model description

The SW radiative transfer model used is described in detail in the work by Hatzianastassiou et al. (2004a), where it has been used to compute the top of atmosphere (TOA) SW radiation budget. It was developed from a radiative-convective model (Vardavas and Carver, 1984) and other versions have been used by Vardavas and Koutoulaki (1995) and Hatzianastassiou and Vardavas (1999, 2001) to compute the SW radiation budget of northern and southern hemispheres on a mean monthly and 10° latitude zonal basis. The model has been successfully tested (cf. Hatzianastassiou and Vardavas, 1999, 2001) according to the Intercomparison of Radiation Codes in Climate Models (ICRCCM) program, as well as against Earth Radiation Budget Experiment (ERBE) S4 scanner data (cf. Hatzianastassiou et al., 2004a).

In brief, the radiative transfer model divides the SW radiation into two spectral bands, one for the ultraviolet-visible (UV-visible) wavelengths ($\lambda < 0.85\,\mu m$) accounting for about 60% of total solar radiation, and a second band for the near-infrared (near-IR) wavelengths ($0.85\,\mu m \leq \lambda \leq 5\,\mu m$) accounting for about 40% of total solar radiation. The model achieves a compromise between accuracy of spectral model computations and speed of computation of parameterisation schemes. The monthly mean incoming total solar flux at TOA for each 2.5-degree latitude-longitude pixel, is computed theoretically, in the way explained in detail by Hatzianastassiou et al. (2004a). The computed incoming solar radiation at TOA for each month and 2.5-degree pixel was compared successfully against 5-year scanner S4 data from ERBE (model – ERBE differences within $2.5\,\mathrm{Wm^{-2}}$) and is divided into the UV-visible and near-IR spectral bands. The solar radiative transfer in the Earth-atmosphere system is treated separately in each spectral band and accounts for absorption and multiple scattering. The model takes into account the physical parameters and processes that affect significantly the solar radiation transfer: ozone (O_3), water vapour (H_2O), carbon dioxide (CO_2), aerosol par-

EGU

ticles, Rayleigh scattering, surface reflection and clouds (low, middle and high-level). For each pixel, the sky is divided into clear and cloudy fractions, and hence direct and diffuse components are considered for solar radiation. The transfer of solar radiation in the Earth-atmosphere system is treated separately for clear- and cloudy-sky atmospheric conditions, by taking into account the presence of the relevant surface and atmospheric parameters (for details see Hatzianastassiou et al., 2004a). The net incoming solar radiation at TOA (planetary absorption), $F_{net,top}^{\downarrow}$, the outgoing SW radiation (OSR) at TOA, $F_{top}^{\uparrow}$, and the planetary albedo R_p, are computed from

$$F_{net,top}^{\downarrow} = \alpha_p F_{top}^{\downarrow} \tag{1}$$

$$F_{top}^{\uparrow} = \left(1 - \alpha_p\right) F_{top}^{\downarrow} \tag{2}$$

$$R_p = \frac{F_{top}^{\uparrow}}{F_{top}^{\downarrow}} \tag{3}$$

where α_p is the planetary absorptivity. The α_p, and hence the OSR (Eq. 2), has a clear-sky component, α_s, and three cloudy-sky components (corresponding to low, middle and high-level clouds), α_{ci}, and is expressed as

$$\alpha_p = (1 - A_c)\,\alpha_s + \sum_i A_{ci}\alpha_{ci} \tag{4}$$

Both clear- and cloudy-sky components are computed by dividing the incoming solar radiation into UV-visible and near-IR components, based on estimated transmissivities, absorptivities, and reflectivities of the different atmospheric and cloud layers and the Earth's surface (see Vardavas and Koutoulaki, 1995; Hatzianastassiou and Vardavas, 1999, 2001). The reflectivity, transmissivity and absorptivity of each atmospheric layer, due to O_3, CO_2, water vapour, and Rayleigh scattering, are computed by using parameterisations derived from laboratory measurements (Vardavas and Koutoulaki, 1995).

Full Screen / Esc

Print Version

Interactive Discussion

EGU

More specifically, absorption by O_3 in the visible between 0.45 and 0.85 μm (Chappuis bands) is taken into account by the model. The O_3 layer also absorbs UV radiation between 0.2 and 0.35 μm (Hartley-Huggins bands). The absorption of solar radiation by CO_2 takes place throughout the atmosphere. We neglect the UV absorption by CO_2, which occurs below 0.2 μm, where the solar flux is less than 0.01% of the total incoming solar flux, while CO_2 absorption in the near-IR is accounted for in the model. The water vapour absorption, which has significant bands in the near-IR, is parameterised in the model as in Vardavas and Koutoulaki (1995).

For each cloud and aerosol layer, computations are performed using two-stream approximation for purely scattering clouds in the UV-visible, and a modified two-stream approximation allowing for cloud absorption in the near-IR (Vardavas and Koutoulaki, 1995; Hatzianastassiou and Vardavas, 1999) and for aerosol absorption in the UV-visible. For clear sky, Rayleigh scattering is taken into account by the model in the UV-visible, while it is neglected for the near-IR component, given that the Rayleigh scattering cross-section decreases rapidly with wavelength. For a cloudy sky, Rayleigh scattering is neglected since cloud optical depth is much larger than the Rayleigh scattering optical depth.

Reflection of incident solar radiation from the Earth's surface is taken into account and the surface reflectivity, R_g, for each 2.5-degree pixel, is computed considering four general types of surface: land, ocean, snow and ice (frozen ocean). Then

$$R_g = f_{land}R_{land} + f_{ocean}R_o + f_{snow}R_s + f_{ice}R_i \tag{5}$$

where f_i is the fractional coverage of the pixel's surface by each type –i of reflecting surface. The ocean reflectivity, R_o, is computed using Fresnel reflection corrected for a non-smooth surface for an incident angle $\phi = \cos^{-1}\mu$ from

$$R_o = 0.5 \left[\left(\frac{\sin a}{\sin b}\right)^2 + \left(\frac{\tan a}{\tan b}\right)^2 \right] + 0.016\cos\varphi \tag{6}$$

where

$$a = \varphi - \sin^{-1}\left[\sin\varphi/1.333\right] \tag{7}$$

$$b = 2\varphi - \alpha \tag{8}$$

For incident solar radiation onto a perfectly smooth water surface, the angle of reflection
5   equals that of incidence, and for normal incidence the reflectivity is 0.021. For an ocean
we correct the Fresnel reflectivity to take into account surface roughness, which leads
to a higher surface reflectivity of about 0.04 for incident solar radiation normal to the
water surface (Kondratyev, 1973). The correction factor $0.016\cos\phi$ goes to zero when
the radiation is parallel to the ocean surface in order to maintain a Fresnel reflectivity
10 of unity in this case. Furthermore, we include the condition that if Fresnel reflectivity
is greater than ice- or snow reflectivity, which occurs for low solar elevations, then
the reflectivities of ice or snow are set equal to the Fresnel one. Kuhn (1989) gives
observations that clearly show this behaviour for snow cover in Antarctica.

Snow albedo, R_s, is set equal to 0.85 and 0.65 (Dickinson et al., 1993) in the UV-
15 visible and near-IR, respectively, while sea-ice albedo, R_i, is set equal to 0.7 and 0.5
(Roesch et al., 2002) in the UV-visible and near-IR, respectively, based on recent es-
timates. Given that land shows a strong spatial variability in terms of its type and as-
sociated reflectance values, the data used were derived from ERBE data for clear sky,
while overcast albedos were obtained by modifying the corresponding clear-sky values
20 for diffuse radiation conditions (Darnell et al., 1992). Alternatively, the land surface
albedo was also computed based on information on land cover, taken from the Inter-
national Satellite Land Surface Climatology Project (ISLSCP, Sellers et al., 1995). The
ISLSCP data were produced for the 24-month period (1987–1988) and are mapped to
$1°$ by $1°$ spatial resolution, with a mean monthly temporal resolution. They describe
25 the geographical distribution of major cover types, based on inter-annual variation of
Normalized Difference Vegetation Index (NDVI). Information for fractional coverage for
each surface type (land, ocean, snow, ice) is obtained from ISCCP-D2 data (Rossow
et al., 1996), whereas suitable reflectivity values for each surface type are ascribed,

**Earth's surface
shortwave radiation
budget**

N. Hatzianastassiou et al.

Title Page

Abstract	Introduction
Conclusions	References
Tables	Figures

◄◄   ►►

◄   ►

Back   Close

Full Screen / Esc

Print Version

Interactive Discussion

EGU

based on values taken from literature (Henderson-Sellers and Wilson, 1983; Briegleb et al., 1986), which allow for spectral dependence over the UV-visible and near-IR range of wavelengths, which is very important (Wei et al., 2001), but also allow for different values for the direct and diffuse components of solar radiation. A correction was applied to land-surface albedo for high-altitude mountainous areas such as Tibet, Rocky Mountains or Antarctica's plateau, consisting in a reduction of the albedo, in order to take into account the decrease of R_g over mountainous non-forested areas, especially during winter, due to the sub-grid orography (Roesch et al., 2001).

The downward SW radiation at the Earth's surface (DSR) and the net downward (or absorbed) SW radiation at surface, are finally computed from the incoming SW radiation at TOA, $F_{top}^{\downarrow}$, in terms of an effective atmospheric transmissivity, t^*, with components t_s^* and t_{ci}^*, for a clear-sky and cloudy sky covered by cloud type $-i$, respectively,

$$DSR = t^* \cdot F_{top}^{\downarrow} \tag{9}$$

where

$$t^* = (1 - A_c) \cdot t_s^* + \sum_i A_{ci} \cdot t_{ci}^* \tag{10}$$

The effective atmospheric transmissivities t_s^* and t_{ci}^* are computed from estimated transmissivities of ozone, Rayleigh, water vapour, carbon dioxide, aerosols, and low, middle and high-level clouds, as well as reflectivities of surface, clouds and Rayleigh, as given by Vardavas and Koutoulaki (1995).

3. The model data

3.1. Ozone, carbon dioxide and water vapour

The mean monthly 2.5-degree latitude-longitude pixel data of the total O_3 column abundance (in Dobson Units) covering the years 1984–2000, were taken from TOVS,

Earth's surface shortwave radiation budget

N. Hatzianastassiou et al.

archived in the ISCCP-D2 package. For CO_2 a fixed total atmospheric amount was taken, equal to 0.54 g cm^{-2}, corresponding to 345 parts per million by volume (ppmv). The water vapour data used were taken from both the NCEP/NCAR and ECMWF Global Reanalysis Projects, which provide long-term climatological data. The data for specific humidity and atmospheric temperature were used to compute the total atmospheric water vapour content, W_{H2O}. The gridded NCEP/NCAR and ECMWF data are provided at surface and various atmospheric levels that extend from the surface up to the stratosphere. Relative humidity data were also used to compute the humidity of the aerosol layer. The differences, arising from the use of the two data sets, in terms of surface SW radiative fluxes were found to be small (mostly within 1–2 Wm^{-2} at pixel level), as discussed in Sect. 4.

3.2. Clouds

Mean monthly cloud properties on 2.5-degree equal-angle pixel resolution for the study period (1984–2000) were taken from the latest D2 stage data of ISCCP (Rossow et al., 1996; Rossow and Schiffer, 1999), which are improvements over the previous C-series version (Rossow and Schiffer, 1999). Cloud properties are provided from ISCCP for nine (9) cloud types which are grouped into three categories: low-level clouds having top pressures greater than or equal to 680 mbar, high-level clouds with top pressures less than 440 mbar and mid-level clouds in between (Rossow et al. 1996). Low-level clouds are considered to be Cu, St and Sc clouds. The middle ones include Ac, As and Ns, while Ci, Cs and deep-convective clouds are considered as high-level clouds. High clouds are treated as cold clouds, while each of the above low and middle clouds are subdivided into liquid- or ice-phase clouds, resulting in 15 cloud types for which properties such as cloud cover, cloud optical thickness, cloud-top temperature and pressure, as well as liquid or ice water path are provided by ISCCP-D2. The values for the 15 independent cloud types were then appropriately averaged (see Hatzianastassiou and Vardavas, 1999) to yield data for low, mid and high-level clouds needed by our model. Note that in our study, the ISCCP-D2 individual cloud data are used, which are derived

by using the visible/infrared (VIS/IR) analysis, rather than the low, mid and high-level cloud data, also provided by ISCCP-D2, which are derived by using the IR-only analysis. This was done because the combined VIS/IR analysis is superior to the IR-only during daytime (Rossow et al., 1996), which is more appropriate for SW radiation budget studies. The VIS/IR (individual) cloud data were found to dramatically improve the model results at both TOA and surface, in terms of comparison with ERBE-S4 satellite and BSRN and GEBA site measurements, respectively.

Cloud cover fractions, A_{ci}, for low, mid, and high clouds are calculated from the sum of cover fractions of the independent ISCCP-D2 cloud types, whereas the total cloud cover fraction, A_c, is calculated from the sum of fractions for low, middle and high clouds

$$A_c = \sum_i A_{ci} \qquad (11)$$

For the computation of the cloud SW transmissivity and reflectivity, the model also requires cloud absorption optical depth, τ_c^a, and cloud scattering optical depth, τ_c^s. ISCCP-D2 provides, however, τ_c^s only at the visible wavelength 0.6μm. The τ_c^s(near-IR) and τ_c^a(near-IR) values were derived by using either Mie computations or existing parameterisations (Slingo, 1989; Ebert and Curry, 1992) for ISCCP-D2 liquid and ice clouds, by assuming the appropriate ISCCP-D2 cloud microphysics, as explained in detail by Hatzianastassiou et al. (2004a). For the computation of cloud reflectivity and transmissivity, the model needs values for the cloud asymmetry parameter, g_c, not provided by ISCCP, which differ between liquid and ice clouds (Liou, 2002). Thus, values of g_c were computed separately for liquid and ice clouds, for both UV-visible and near-IR range of wavelengths, by using both Mie computations and parameterisations, as explained by Hatzianastassiou et al. (2004a). The computed g_c values in the UV-visible are equal to 0.85 and 0.78 for liquid and ice clouds, respectively, while the corresponding values in the near-IR range are equal to 0.82 and 0.8.

3.3. Rayleigh scattering, surface reflection and aerosol particles

Rayleigh scattering is considered in the model as described in Vardavas and Koutoulaki (1995). The surface reflection is computed with the model at each pixel for each month in the period 1984–2000, by considering four types of surface: land, ocean, snow, and ice (frozen ocean). Information on spatial and temporal variation of the fractional coverage of the Earth's surface by each type, was taken from ISCCP-D2. The radiative effect of aerosols is computed with our model by using a modified two-stream approximation allowing for scattering and absorption in the UV-visible and near-IR ranges of wavelength. Our model requires aerosol optical properties, namely aerosol optical thickness (AOT), single scattering albedo (ω_{aer}), and asymmetry parameter (g_{aer}). Currently, there is no data base providing such aerosol data for the whole study period 1984–2000 on a global scale. There are new satellite-based instruments (e.g. Moderate Resolution Imaging Spectro-Radiometer, MODIS, or Polarization and Directionality of the Earth's Reflectance, POLDER) performing accurate spectral aerosol measurements on a global scale, but they have only started their operation from year 2001. There are some AOT data for the whole period from the Global Aerosol Climatology Project (GACP), but without global coverage as they only cover the ocean areas. On the other hand, there are AOT data with global coverage from the Total Ozone Mapping Spectrometer (TOMS, Torres et al., 2002), but no ω_{aer}, and g_{aer} data. New re-processed AOT data from TOMS, including ω_{aer} data, that will cover the period 1979–2000 will be released by NASA Goddard Space Flight Center (GSFC). In the meantime, as a first step, the model-required aerosol data were derived from the Global Aerosol Data Set (GADS, Koepke et al., 1997). GADS provides AOT, ω_{aer}, and g_{aer} data, at 61 wavelengths from 0.25 to 40 μm, 27 of which lie in the SW range, and for 8 values of relative humidity (0, 50, 70, 80, 90, 95, 98, and 99%). Given the strong dependence of aerosol optical properties on ambient relative humidity, the original GADS properties were then re-computed in a realistic way, for actual relative humidity values for the aerosol layer, as explained in detail by Hatzianastassiou et

Earth's surface shortwave radiation budget

N. Hatzianastassiou et al.

EGU

al. (2004b) for each month in the period from January 1984 to December 2000. Subsequently, the computed values of aerosol optical properties were averaged into the UV-visible and near-IR ranges, weighted by the spectral distribution of the incoming solar flux (Thakaekara and Drummond, 1971). A complete description of the treatment of aerosols in the model, as well as of GADS aerosol data, can be found in the work by Hatzianastassiou et al. (2004b).

3.4. Cloud-top pressure, cloud physical thickness and surface pressure

The cloud-top pressure, p_c, and physical thickness, dp_c, both determine the atmospheric layer where water vapour absorption is replaced by cloud scattering and absorption. Values of p_c were taken from ISCCP-D2 for low, mid, and high-level clouds. The ISCCP-D2 does not provide dp_c data, so these were estimated from Peng et al. (1982) for the Northern Hemisphere, as explained in the work by Hatzianastassiou and Vardavas (1999), while dp_c values for Southern Hemisphere were estimated in the way described by Hatzianastassiou and Vardavas (2001), by combining the values from Peng et al. and those derived from Liou (1992). A complete topography scheme (which is important for regions with high altitude, such as the Tibetan plateau, Antarctica, Rocky or the Andes mountains) is included in the model, which uses surface pressure, p_s, data taken either from NCEP/NCAR or from ECMWF Global Reanalysis Projects gridded in 2.5° by 2.5° pixels for each month of the 17-year period 1984–2000.

4. Model results

4.1. Seasonal and geographical distributions

The geographical distribution of the 17-year average downward SW radiation (DSR) at the Earth's surface is determined by the incoming SW radiation at TOA, and the scattering and absorption processes taking place within the Earth-atmosphere system, between the solar radiation and surface and atmospheric parameters (clouds,

surface, water vapour, trace gases and particulate matter). The latitudinal gradient of DSR is primarily determined by the incoming solar flux at TOA, and secondarily by clouds, while the patterns of longitudinal variation are mostly determined by cloud and surface properties. Therefore, large DSR fluxes are found in polar regions (Figs. 1a, c) during local summer, equal to about 300–350 Wm^{-2} over Antarctica in January and 200–250 Wm^{-2} over the Arctic in July. Our values are lower than those given by Gupta et al. (1999), which are equal to 400–450 Wm^{-2} in Antarctica and 250–300 Wm^{-2} in the Arctic. Note, however, that Gupta et al. used ISCCP C-series data to derive a 8-year (1983–1991) SRB against our 17-year (1984–2000) averages. The larger values over Antarctica than the Arctic are due to the larger incoming solar radiation at TOA during perihelion (>500 Wm^{-2}), but also to the smaller ISCCP-D2 summer cloudiness in Antarctica than in the Arctic ($\approx$20% against $\approx$60%, respectively). There is a gradual DSR decrease from the summer to winter pole in January and July, leading to zero values poleward of mid-to-high latitudes. The white areas in Fig. 1 correspond to missing ISCCP model input data, but they do not affect our results since they coincide with polar night conditions. The latitudinal gradient of DSR is mitigated during spring and autumn (Figs 1b,d). Overall, the DSR has maximum values over the subsidence regions associated with anticyclonic conditions and small cloud amounts, such as oceanic areas in low latitudes of the summer hemisphere, as well as over the polar areas of the summer hemisphere. In contrast, small DSR values are found over regions with large cloud amounts, such as the middle latitudes of the summer hemisphere. Thus, DSR values as low as 140 Wm^{-2} are found over the storm-track zone of southern hemisphere (50°–70° S) in January, whereas values down to about 100 Wm^{-2} are computed in October. Corresponding features, with DSR values equal to 100–140 Wm^{-2} in April and July, exist over northern Pacific Ocean's areas with large cloud amounts (equal to about 90%). In general, there is a strong anti-correlation between DSR and cloud amount. Note the small DSR values off the western coasts of South America and South Africa in July, being smaller than corresponding DSR fluxes in adjacent regions of the same latitude, which are attributed to large cloud amounts (of about 80%). Also, note the relatively

Earth's surface shortwave radiation budget

N. Hatzianastassiou et al.

Title Page

Abstract | Introduction

Conclusions | References

Tables | Figures

◀ | ▶

◀ | ▶

Back | Close

Full Screen / Esc

Print Version

Interactive Discussion

EGU

small DSR values over south-eastern Asia in July ($\approx$150 Wm^{-2}), where large cloud cover ($\approx$80%) exists, associated with monsoons. Apart from oceanic areas, there are some extended continental regions with large DSR values, such as the United States, South Europe, North Africa and middle-East in April and July, or South America, South Africa and Australia in January and October. In general, the distribution of DSR has very similar patterns with the outgoing SW radiation (OSR) at TOA (see Hatzianastassiou et al., 2004a), but with inverted minimum/maximum values. For example, the relatively small DSR fluxes over the equatorial regions, caused by the cloudiness along the inter-tropical convergence zone (ITCZ), are opposite to the relatively large OSR fluxes there (Hatzianastassiou et al., 2004a).

The net DSR fluxes, given in Figs. 2a–d, are very similar to the DSR fluxes. Over oceanic areas, with a small albedo, the differences are quite small, while the most important differences are found over the highly reflecting surfaces, such as deserts or snow- and ice-covered polar areas, having surface albedo values reaching 40 and 95%, respectively, leading thus to small net DSR values ($<$100 Wm^{-2}) over Antarctica in January and the Arctic in July (the corresponding DSR values are about 350 and 250 Wm^{-2}). This is clearly illustrated by a comparison between the north African desert and the adjacent Mediterranean Sea for July (Fig. 2c), which shows differences of about 125–150 Wm^{-2}, while there are no significant differences in DSR fluxes (Fig. 1c).

Latitude zonal averages, over the 17-year period from January 1984 to December 2000, of monthly mean DSR and net DSR fluxes (Figs. 3a, b), show that DSR fluxes vary from zero to 375 Wm^{-2}, having maxima over sub-tropical and polar areas of both hemispheres in summer, of about 310 and 370 Wm^{-2}, respectively. The maximum values at the South Pole are slightly larger than those of the North Pole, due to the slightly smaller Earth-Sun distance, smaller cloudiness and drier atmosphere. Small seasonal variations exist in the tropics, where weak seasonal variation in solar declination and cloudiness occur. The seasonal variability of DSR increases towards the poles, where it can be up to 375 Wm^{-2}. Large DSR values are found in northern hemispherical areas extending from the equator to the North Pole in July, whilst in the southern hemisphere

in January, there are relatively smaller DSR fluxes of about $150\,\mathrm{Wm^{-2}}$ from $50°$ S to $70°$ S, due to large cloudiness along the storm-track zone of South Hemisphere. In both hemispheres, the maximum of DSR values occur in sub-tropical areas (between 10 and $35°$ of latitude) rather than in the tropics, apart from the poles. This is due to the fact

5   that total cloudiness has minimum values (of about 50%) over the above sub-tropical areas, and not along the equator, where the ITCZ involves total cloud cover values of about 60–70%, according to the ISCCP-D2 data. Our computed zonally averaged DSR values agree with the corresponding 8-year averages given by Gupta et al. (1999), but they are smaller in the polar areas by $30–80\,\mathrm{Wm^{-2}}$. In the tropics, ($20°$ S–$20°$ N),

10   maximum DSR values occur during spring and autumn, and not in summer as in subtropical, mid-latitude and polar areas. This behaviour, which has been also reported by Darnell et al. (1992) and Hatzianastassiou and Vardavas (1999), is attributed to maximum values in the incoming solar radiation at TOA during these seasons over the tropics, as well as to relevant features in the annual cycle of cloudiness and total precip-

15   itable water. Our maximum DSR and net DSR values in tropical and sub-tropical areas ($20°$ S–$20°$ N) are slightly larger (by $\approx 10\,\mathrm{Wm^{-2}}$) than those given by Hatzianastassiou and Vardavas (1999) and even larger than those of Vardavas and Koutoulaki (1995), while over Antarctica they are smaller than those given by Hatzianastassiou and Vardavas (2001) by $20–30\,\mathrm{Wm^{-2}}$. The zonally averaged values presented here, however,

20   should be more reliable, since the earlier ones were computed using zonal averages of model input data to produce zonal mean fluxes, rather than pixel-level input data. Although the net DSR fluxes (Fig. 3b) show some similar features with the DSR values, there are also some differences. Thus, the polar areas do not show maxima in net DSR fluxes, while there is a significant inter-hemispherical contrast in terms of the magni-

25   tude of summer sub-tropical maximum net DSR values, due to the smaller surface albedo of the South Hemisphere (smaller land-to-sea ratio).

[EGU](#)

4.2. Time series

The time series of global zonally averaged monthly mean DSR and net DSR fluxes over the entire 204-month period 1984–2000 indicate that the patterns shown in Fig. 3 are repeated over the 17-year period (Fig. 4). Thus, maximum DSR values of about 260–280 Wm^{-2} occur over sub-tropical regions (10°–40° N and S) during local summer, whereas maximum values are also found in polar areas during summer, which are slightly larger in the southern than northern pole. Local minimum values of about 200 Wm^{-2} are found in equatorial areas, induced by the ITCZ cloudiness, as well as over both hemispherical middle-to-high latitudes (around 60° N and S), due to the large stratiform cloud amounts over the oceans at these latitudes. The features of net DSR are very similar to those of DSR, except in polar areas, where the net DSR drops down to values of <100 Wm^{-2}. Although there are some inter-annual trends in the surface SW radiation fluxes, these cannot be clearly seen in plots such as those in Figs. 4a, b, because of the extended scale of values.

The time-series of the mean monthly hemispheric and global average components of the surface SRB, over the entire 204-month period from 1984 to 2000, reveal a strong seasonal cycle for the hemispheric averages of DSR (Fig. 5a). The South Hemisphere has a slightly larger amplitude ($\approx$125 Wm^{-2}) than the North one ($\approx$110 Wm^{-2}). This is due to the fact that the seasonal cycle of the net incoming SW radiation at TOA is larger in the South Hemisphere ($\approx$300 Wm^{-2}) than in the North one ($\approx$250 Wm^{-2}). Another reason is that, as shown by our analysis using both NCEP/NCAR and ECMWF data, the total precipitable water of the Northern Hemisphere shows a stronger seasonal cycle than that of the Southern Hemisphere, with very large values (up to $\approx$3.2 g cm^{-2}) in July, against values of about 2.8 g cm^{-2} in the South Hemisphere, as also reported by Wittmeyer and Vonder Haar (1994). Therefore, the summer-maximum of DSR in the South Hemisphere reaches about 240 Wm^{-2}, against 230 Wm^{-2} in the North one. The hemispherical DSR averages balance each other to produce a monthly mean global average DSR with a small seasonal variability ($\approx$10–20 Wm^{-2}), with pri-

EGU

mary and secondary maxima and minima. The applied linear regression to the mean global DSR 17-year time-series, shows an increasing trend in DSR, equal to $4.1\,\mathrm{Wm}^{-2}$ over the time period 1984–2000, which is equivalent to a decadal increasing trend of $2.4\,\mathrm{Wm}^{-2}$. This increasing trend in DSR is associated with a 17-year decreasing trend in the reflected SW radiation at TOA, equal to $3.2\,\mathrm{Wm}^{-2}$, as shown by Hatzianastassiou et al. (2004a). Our analysis has shown that the trends in both DSR and OSR are not attributed to the incoming SW radiation at TOA, since the latter shows an insignificant trend of $0.1\,\mathrm{Wm}^{-2}$, but they are attributed to internal physical processes of the Earth-atmosphere system. Apart from DSR, the net DSR flux has also increased by $3.7\,\mathrm{Wm}^{-2}$ over the 17-year period from 1984 to 2000 (or by $2.2\,\mathrm{Wm}^{-2}$ on a decadal scale).

We have performed an analysis that shows that the increasing trend in global mean DSR arises, to a large extent, in tropical and sub-tropical areas. Therefore, our study indicates that the change in tropical SW radiation budget at TOA (increasing planetary heating), indicated by both satellite observations (Wielicki et al., 2002) and model computations (Hatzianastassiou et al., 2004a; Fotiadi et al., 2005) is associated with a significant increasing surface solar radiative heating, involving enhancements in both downward and absorbed solar radiation at the Earth's surface, especially in low latitudes. It should be noted that since the long-term increase in net DSR ($3.7\,\mathrm{Wm}^{-2}$) exceeds the corresponding long-term decrease in OSR ($3.2\,\mathrm{Wm}^{-2}$), there must be a long-term decrease in SW atmospheric absorption (cooling) by $0.5\,\mathrm{Wm}^{-2}$, verified by our study. Overall, our modelling study indicates that over the 17-year period from 1984 to 2000, a significant change in the SW radiation budget has taken place, consisting in a planetary solar heating, resulting from a stronger surface solar heating combined with a smaller atmospheric solar cooling. This should have affected the atmospheric dynamics by strengthening the Hadley and Walker circulations (Chen et al., 2002), altering the atmospheric temperature gradient and the formation of clouds and precipitation. Of course, further and more detailed investigations are necessary to draw definite conclusions. For example, the model results, in terms of DSR and net DSR

EGU

Earth's surface shortwave radiation budget

N. Hatzianastassiou et al.

trends, have to be inter-compared with corresponding trends in station measurements, and a relevant work is in preparation. Besides, the reasons of the apparent increasing trend in DSR need to be more thoroughly investigated. A preliminary analysis was performed, in which the correlation coefficients between long-term tendencies in DSR and various physical parameters that determine DSR, were computed. In our model these parameters are: cloud (low, middle and high-level) cover, cloud scattering and absorption optical depths, surface albedo, total precipitable water, total column O_3 concentration and incoming SW radiation at TOA. The results of our analysis show that a decrease in cloud cover, especially low-level, is primarily responsible for the increasing trend in DSR. We have also performed another study in which we have computed the contribution of each one of the above relevant physical parameters to the computed trends in DSR and net DSR, as in the works by Hatzidimitriou et al. (2004) and Fotiadi et al. (2005). The results of this analysis show that about 70% of the total trend in surface solar radiation comes from the low-level clouds. The results of these preliminary analyses are in line with similar studies performed to investigate the physical sources of the corresponding decreasing trend in OSR (Hatzianastassiou et al., 2004a).

The computed anomalies in hemispherical mean DSR fluxes over the 17-year period (1984–2000), vary from -9 to $9\,\mathrm{Wm}^{-2}$ (Fig. 6a), while the global mean DSR anomaly has variations of up to $6\,\mathrm{Wm}^{-2}$, about the 17-year mean value. Large negative anomalies, i.e. decreased SW radiation reaching the Earth's surface, are found for the period 1991–1993, which can be attributed to the Mount Pinatubo eruption in June 1991, and to the 1991/1992 El Niño event. During the same period, the outgoing SW radiation has drastically increased by about $4\,\mathrm{Wm}^{-2}$ (see Hatzianastassiou et al., 2004a). The induced rapid decrease in DSR is followed by a recovery period, with positive DSR anomalies through 1994. There are also other interesting features corresponding to climatic events, such as El Niño and La Niña, associated with negative and positive DSR anomalies, respectively. For example, negative DSR anomalies as large as $6\,\mathrm{Wm}^{-2}$ follow the 1986/1987 El Niño event (Fig. 6a). The large negative DSR anomalies of about $-5\,\mathrm{Wm}^{-2}$ during 1984 can be attributed to the influence of the El Chichon erup-

tion that took place in 1983. Also, note that in 1998 the DSR anomalies pass from large positive values (of about $4\,\mathrm{Wm}^{-2}$) to negative ones (equal to $-2\,\mathrm{Wm}^{-2}$), which can be attributed to the 1997/1998 El Niño event. In general, the variation of DSR anomalies is similar but opposite in magnitude to that of OSR anomalies (see Hatzianasassiou et al.,

5 2004). The 4th order polynomial fit to 17-year time-series of global averages of DSR anomalies shows significant positive DSR anomalies (increasing DSR) in the period starting from year 1992 (Fig. 6). On the contrary, in the period 1984–1992, negative DSR anomalies mostly occur, indicating a decreasing DSR flux at the Earth's surface. This is in agreement with most measurements and modelling studies, reporting a de-

10 creasing trend in DSR during the period between 1960 and 1990 (e.g. Gilgen et al., 1998; Stanhill and Cohen, 2001; Liepert, 2002; Wild et al., 2004). Our model results, however, show that the situation has changed after the early 1990s, since the surface solar radiation is found to have increased, due to a decrease in cloudiness, especially low-level, primarily in tropical and sub-tropical regions. Thus, it seems that during the

15 last decade of the 20th century, the effect of clouds has dominated any other effect. This is expected, given that surface solar radiation is more sensitive to clouds rather than other physical parameters, within the range of their natural variability (cf. Sect. 5).

4.3. Mean annual, hemispherical, and global surface SW radiation budget components

20 Monthly mean 10-degree latitude zonal fluxes were computed by averaging first along 2.5°-width longitudinal circles, then along latitude, by considering the fraction of surface area contained in each 2.5-degree zone. Subsequently, annual mean quantities were computed by summing the corresponding monthly means for each 10-degree latitudinal zone over the 12 months of the year. The latitudinal variation of mean annual

25 DSR flux has maximum values of about $230\,\mathrm{Wm}^{-2}$ in sub-tropical areas, while it drops rapidly to about $80\,\mathrm{Wm}^{-2}$ towards the poles (Fig. 7a). The equator-to-pole variation in DSR is primarily determined by the latitudinal variation of solar zenith angle, but it is also influenced by cloudiness. Thus, there is a local minimum in mean annual DSR

in the equator (equal to about 220 Wm^{-2}), which is caused by clouds associated with the ITCZ. There is a local maximum of 230 Wm^{-2} in DSR around 15° N, in agreement with previous studies (Liou, 1992; Hatzianastassiou and Vardavas, 1999) while Darnell et al. (1992) reported a similar local maximum, but shifted poleward by 10° latitude.

5 Note that in the South Hemisphere, there are local minimum and maximum DSR values around 60° S and at the south pole, respectively, while in the North Hemisphere there is a continuous equator-to-pole decrease in DSR. The local minimum in DSR around 60° S, is caused by the persistent and extended cloudiness occurring over the oceanic zone of South Hemisphere, and underlines the very important role of clouds,

10 apart from that of solar declination, in determining the DSR fluxes. The net DSR flux decreases from about 210 Wm^{-2} in the tropics to 20–30 Wm^{-2} in the polar regions (Fig. 7b). It is very similar to DSR (for example it has local sub-tropical maximum values), except for the polar areas, but it has differences as well. Thus, the local minimum in DSR near 60° S, does not exist in the mean annual net DSR flux, since it is

15 smoothed out by the much larger absorption of DSR by the Antarctic ocean than the adjacent Antarctic continent. Note that in contrast to larger DSR fluxes over Antarctica than the Arctic (Fig. 7a), there are slightly smaller net DSR fluxes, due to Antarctica's larger surface albedo. Our values in the tropics are smaller by 5–10 Wm^{-2} than those given by Hatzianastassiou and Vardavas (1999). Also, our net DSR values are found

20 to be at the lower end of the range of values given by Li et al. (1997), based on various observational and modelling estimates, in both tropical and polar areas.

The mean hemispherical DSR fluxes have opposite seasonalities, varying within the range 110–230 Wm^{-2}, resulting thus in a mean global DSR flux ranging from 165 to 176 Wm^{-2} throughout the year (Fig. 7c). The corresponding seasonal variation in

25 global mean net DSR flux is equal to 8 Wm^{-2} (Fig. 7d). There is a smaller seasonal variation in net DSR than DSR for both hemispheres and the globe, which is attributed to the effect of surface albedo. Nevertheless, for both DSR and net DSR, the seasonal variability is slightly larger in the southern than in the northern hemisphere, which can be attributed to the larger seasonal variation of the incoming SW radiation at TOA in

the southern hemisphere (Hatzianastassiou et al., 2004a). The northern hemispherical mean net DSR fluxes are smaller than the corresponding values given by Hatzianastassiou and Vardavas (1999) by 10 and 15 Wm^{-2}, in terms of their winter minimum and summer maximum values.

The mean annual hemispherical and global average values over the 17-year period from 1984 to 2000, for the downward and net downward (i.e. absorbed) SW radiation at surface, along with corresponding values for the 4 mid-seasonal months of the year, are given in Table 1, while in Table 2, our computed DSR and net DSR values are also intercompared with other published values. Note that very few other studies give both SRB components for the two hemispheres and the globe. On a 17-year basis (1984–2000), the Earth's surface is found to receive 171.6 Wm^{-2} and to absorb 149.4 Wm^{-2}, resulting in a long-term surface albedo equal to 12.9%. The inter-hemispherical differences are equal to 4.6 Wm^{-2} for DSR and only 0.3 Wm^{-2} for net DSR, implying slightly larger northern than southern hemispherical surface solar radiative fluxes. Overall, according to our 17-year model results using ISCCP-D2 data, on a mean annual basis and at global scale, the Earth receives 50.2%, while it absorbs 43.7% of the incoming SW radiation entering the Earth-atmosphere system. Our model-computed values are very close to those given by surface observations (GEBA), with differences equal to 2.6 and 1.6 Wm^{-2} for DSR and net DSR, respectively, while they are significantly smaller than most estimates from other physical deterministic models, GCMs and climatic models, as well as from reanalysis products, by up to 30 Wm^{-2}. In contrast, our model results seem to be close to those of the ECHAM model as well as those of ECMWF-ERA. Note that in previous SRB studies, a significant overestimation of net DSR flux has been reported, with respect to the surface-based estimate given by Ohmura and Gilgen (1993), involving an uncertainty in the knowledge of SRB (Li et al., 1997; Kiehl and Trenberth, 1997) of about 20–25 Wm^{-2}. This overestimation has been associated with extra atmospheric solar absorption (by clouds or aerosols) as indicated by observational studies (Cess et al., 1995; Ramanathan et al., 1995; Pilewski and Valero, 1995), but also verified by modelling studies (Garratt et al., 1998; Wild et

al., 1998; Hinkelman et al., 1999). On the other hand, it has been argued that the surface-based estimate by Ohmura and Gilgen (1993) was probably too low, since it was derived by measurements taken at a limited number of stations, usually located over land areas (Kiehl and Trenberth, 1997) and especially populated ones (Li et al., 1997). Since then, the number of stations involved in GEBA and BSRN networks has increased, and their spatial coverage expanded to cover remote areas, such as Greenland and Antarctica. Recently, the "best" surface-based estimate of surface solar absorption (net DSR) has been revised to 151 Wm^{-2} for net DSR, close to our model computed value of 149.4 Wm^{-2}.

5. Sensitivity of surface SW radiation budget

The assessment and quantification of the role of various physical key parameters that determine the DSR and net DSR fluxes at surface is very important for SW radiation budget studies. To this aim, a series of sensitivity tests were performed with our model. In each test, the relevant parameter, V, was modified by a certain amount, ΔV, i.e. by 10% in most cases, in relative percentage terms, and the modifications of the downward SW radiation at surface, Δ(DSR), and of the net DSR flux at surface, Δ(NDSR), with respect to the defined reference cases, were computed and subsequently expressed either in absolute terms (in Wm^{-2}) or in relative percentage values. The results given in Table 3 provide values in absolute terms. The year 1988 was chosen to represent the reference case. The tests were performed on a monthly basis and at the pixel level, but results are given here in terms of globally and annually averaged Δ(DSR) and Δ(NDSR) absolute values. Our model sensitivities are valuable for assessing possible sources for the obtained discrepancies between model-computed and surface-measured DSR and net DSR fluxes. The results of our model sensitivity tests indicate that, on a mean annual and global basis, DSR is found to be primarily sensitive to cloud parameters, namely the cloud cover, cloud optical depth (especially the scattering one), cloud asymmetry parameter, as well as to total precipitable water.

EGU

Increasing A_c by 10%, separately for low, middle, or high-level clouds, resulted in a decrease of DSR by up to $3.2\,\text{Wm}^{-2}$ (or about 2%). The DSR fluxes were found to be more sensitive to low rather than to middle or high-level clouds. This is also valid for the sensitivity of DSR to τ_c^s; thus, increasing τ_c^s by 10% reduced DSR by up to $1.2\,\text{Wm}^{-2}$.

5 Modifying the cloud asymmetry parameter, g_c, by 5% in relative values, modified DSR by as much as $8\,\text{Wm}^{-2}$. This shows that the surface solar radiation is very sensitive to g_c, which justifies the special care that was taken in modelling this cloud parameter in our study. According to our modelling study, changes in the incoming solar radiation at TOA by 1% (or by about $3.5\,\text{Wm}^{-2}$) can modify DSR by $1.7\,\text{Wm}^{-2}$ at the global scale,

10 which is important in terms of possible climatic change due to solar variability. It is interesting that, based on our model sensitivity study, increasing the total precipitable water by 10%, results in a globally averaged decrease in DSR by about $2\,\text{Wm}^{-2}$ (or about 1.1%), which can be important in view of the existing differences between available humidity data from different reanalysis products (e.g. NCEP/NCAR or ECMWF).

15 Much larger Δ(DSR) values are computed on a local scale in our sensitivity tests, as can be seen in Table 3. The sensitivity Δ(NDSR) values are slightly smaller than the Δ(DSR) ones, apart from the case of surface albedo.

In order to investigate the effect of using humidity data from different sources, we have performed another sensitivity study, in which the model was run for the years

20 1985–1993 by using data either from the NCEP/NCAR or the ECMWF ERA-15 reanalysis projects, and compared the resulting DSR fluxes at pixel-level (2.5-degree longitude-latitude) and on a monthly mean basis. The results are given in Fig. 8, where one can see that overall, the DSR fluxes are highly correlated (R=99.96%), with a standard deviation of $2.16\,\text{Wm}^{-2}$ and a very small bias, equal to $0.07\,\text{Wm}^{-2}$, corre-

25 sponding to only 0.04% of the mean annual global DSR flux. This verifies that using NCEP/NCAR or ECMWF data in our model, has generally little impact on the computed DSR fluxes. Using ECMWF data generally leads to larger DSR fluxes than using data from NCEP/NCAR. Nevertheless, our more detailed analysis has shown that somewhat larger differences in DSR are found at the pixel level, although in the majority of

Earth's surface shortwave radiation budget

N. Hatzianastassiou et al.

Title Page

Abstract | Introduction

Conclusions | References

Tables | Figures

◄◄ | ►►

◄ | ►

Back | Close

Full Screen / Esc

Print Version

Interactive Discussion

EGU

cases they do not exceed $2\,Wm^{-2}$. For specific cases, however, DSR differences reach values of $10\,Wm^{-2}$; this is the case over areas with a significant topography, such as the Tibetan plateau, Greenland, Rocky Mountains or the Andes. Over these areas, the ECMWF specific humidity is lower than that of NCEP/NCAR, by up to 10–20 g/Kg,

5   leading thus to larger DSR fluxes.

6.   Comparisons with surface-site measurements

The model computed DSR fluxes have been validated through comparison with corresponding extensive measurements from stations. Such high-quality surface-based data were taken from two sources, namely the Baseline Surface Radiation Network

10   (BSRN, Ohmura et al., 1998) and the Global Energy Balance Archive (GEBA, Gilgen and Ohmura, 1999). The BSRN stations have to follow specific observational and calibration procedures, resulting in standardized data of very high accuracy. The temporal resolution of the data is also exceptional, of the order of minutes. All flux data in the BSRN database are quality checked by WCRP. If more than 80% of the minute val-

15   ues in a specific day pass the quality control, they are subsequently averaged to yield daily values. If this happens for more than 20 days in a month, then monthly values are also computed. We then compare these monthly values with the monthly values calculated by our model. The BSRN network was established in 1992 and the stations from which at least one monthly DSR value in the period 1992–2000 is available, are

20   listed in Table 4. The comparison of observed versus calculated monthly mean DSR fluxes within the 2.5°×2.5° cell containing the BSRN station for all 22 stations, is shown in the scatterplot of Fig. 9a, while the summarised results of model-BSRN comparison, in terms of bias, root mean square error (RMS) and the slope of the least-squares line, for each station, are also listed in Table 4.

25   The scatterplot shows a bias equal to $-14\,Wm^{-2}$, with a relatively small scatter (RMS equal to $30.6\,Wm^{-2}$). A more detailed analysis of the results of model validation against BSRN, shows that the biases do not exceed $10\,Wm^{-2}$ in tropical and mid-latitude areas

of both hemispheres, while the corresponding RMS values remain smaller than about 20 Wm^{-2}. Despite this quite good model performance, there is some underestimation of DSR fluxes with respect to BSRN in stations situated in southern polar areas (67°–90° S), as can be seen in Table 4. This was also found by comparison against GEBA

5 DSR data (Fig. 9b). Nevertheless, note that similar underestimation features of surface solar radiation fluxes with respect to site measurements in polar areas, have been reported also by others (e.g. Wild et al., 1998a, 2004; Wild and Ohmura, 1999). The largest biases and RMS values are found at the stations of Syowa and Neumayer, along Antarctica's coast. Also, the least square line slope is significantly less than

10 unity in these stations, in contrast to values very close to unity for the rest of stations. However, the South Pole station shows much less underestimation and a least-squares line slope equal to one. This is evidence that the model underestimates DSR in the Antarctic coast not because of model deficiencies related to the polar climate, but more likely because of errors in model input data. Since the detection of clouds is problematic

15 over highly reflecting surfaces, such as the poles, and the good model performance at the South Pole station, it seems that clouds might not be the problem. Given that over Antarctica's coastal areas, the model also underestimates OSR (see Hatzianastassiou et al., 2004a), the situation is rather puzzling, and certainly a more detailed analysis is necessary, including careful check of the site measurements. Apart from a few stations,

20 the model generally underestimates DSR with respect to BSRN, resulting thus in an overall negative bias, though small. Examination of the seasonal behaviour of our model performance against BSRN, shows that generally, zero bias is within the error bars, except for the polar regions during summer, and most of the year in the southern mid-latitude areas.

25 A similar comparison of measured against model computed DSR fluxes is performed using another DSR database, the Global Energy Balance Archive (GEBA, Gilgen and Ohmura, 1999). The GEBA contains quality checked monthly means of energy fluxes at the Earth's surface from sites all over the world. Data stored in the GEBA database have been extracted from periodicals, monographs, data reports, and unpublished

manuscripts. About 700 stations with at least one monthly DSR value in the period 1984–2000 were used in the validation of our model. In Fig. 9b is shown the scatterplot comparison of all monthly measured values against the computed values in the 2.5°×2.5° pixel containing the specific GEBA station. Similarly to the BSRN comparison, our model underestimates DSR in the polar areas, but everywhere else the agreement is very good, with an overall bias equal to $-6.5\,\mathrm{Wm^{-2}}$ and a RMS value of $23.5\,\mathrm{Wm^{-2}}$. The GEBA polar stations show that our model underestimates the DSR, similarly to the BSRN stations, but GEBA, in contrast to BSRN, does not show any evidence of DSR underestimation in the southern mid latitudes.

7. Summary and conclusions

A physical deterministic radiative transfer model along with long-term climatological data for various key physical surface and atmospheric parameters, taken from large data bases such as ISCCP-D2, TOVS, GADS, NCEP/NCAR and ECMWF Global Reanalysis projects, have been used to compute the SW surface radiation budget (SRB) for the 17-year period from 1984 to 2000, on a mean monthly basis and 2.5° by 2.5° longitude-latitude pixel resolution at global scale. The model results were validated against quality BSRN and GEBA data for the periods 1992–2000 and 1984–2000, respectively, showing good agreement with surface measurements, with an overall negative bias of 14 and $6.5\,\mathrm{Wm^{-2}}$, with respect to BSRN and GEBA measurements, respectively. The differences between model-computed and surface-measured DSR fluxes, are within $10\,\mathrm{Wm^{-2}}$ at most stations, i.e. close to the uncertainty of BSRN and GEBA data, except for two stations along Antarctica's coast, where systematically larger differences in DSR fluxes were found. Uncertainties in model input data are assessed to be the most likely source for this model DSR underestimation, whereas similar underestimation features at the same stations have been reported by other modelling studies, suggesting also an examination of the quality of site measurements.

The 17-year model results indicate that the Earth's surface receives $171.6\,\mathrm{Wm^{-2}}$,

Title Page

Abstract | Introduction

Conclusions | References

Tables | Figures

|◄ | ►|

◄ | ►

Back | Close

Full Screen / Esc

Print Version

Interactive Discussion

EGU

while it absorbs 149.4 Wm^{-2}, values that correspond to 50.2 and 43.7% of the incoming SW radiation at the top of the atmosphere. These values involve a long-term surface albedo equal to 12.9%. Our computed value of 43.7% for the part of solar radiation that is absorbed by the Earth's surface, is smaller than the values given in previous studies,

5 which are larger than 46%. In combination with a long-term planetary albedo equal to 29.6% (Hatzianastassiou et al., 2004a), our modeling study indicates a partial absorption of solar radiation within the terrestrial atmosphere, equal to 26.7%. Our values of 43.7 and 26.7% for the surface and atmospheric absorption of solar radiation, are significantly smaller and larger, respectively, than the corresponding values of about 50

10 and 20%, estimated by earlier studies. Our value of 149.4 Wm^{-2} for the net downward surface solar radiation, is smaller than the values given by other models and reanalysis projects, by at least 10–20 Wm^{-2}, except for versions 4 and 5 of ECHAM GCM and the ECMWF reanalysis. It is very interesting that our model computed value is very close to the revised "best" estimate of about 150 Wm^{-2} from surface measurements.

15 Comparable DSR and net DSR fluxes were computed for the northern and southern hemispheres. The linear regression analysis applied to 204 global averages of monthly mean DSR fluxes, reveals a significant decadal increase in SW radiation reaching the Earth's surface, equal to 2.4 Wm^{-2}, associated with a corresponding decadal increase in surface solar absorption of 2.2 Wm^{-2}, over the 17-year period 1984–2000. The

20 performed analysis has shown that the increasing surface solar heating, indicated by positive DSR and net DSR anomalies, started after the year 1992, and that it has been caused by a significant reduction in cloudiness during the last decade of 20th century. In contrast, mainly negative anomalies are found from 1984 through the early 1990s. A further analysis has demonstrated that the reduction in low-level cloud amounts,

25 accounts for about 70% of the computed increasing trend in DSR. This is consistent with the results of a sensitivity study, showing that the surface SW radiative fluxes are primarily sensitive to cloud parameters, and more specifically to low, middle, and high-level cloud cover (in that order), and secondarily to other parameters, such as total precipitable water.

In the future, it is desirable to use more advanced models to make such computations of SRB using the same or similar input data. This can improve the accuracy of the results, though it involves other problems, for example greatly increasing computing time, which constitutes a problem in case of global scale studies. Further work is undertaken in order to increase the spatial and temporal resolution of the performed study, providing SRB fluxes at 1° by 1° latitude-longitude resolution or on a daily mean basis. Besides, it is very important to perform similar validations of computed SRB fluxes on as long as possible time periods, since SRB changes with time. Of course, this is restricted by the availability of either model computed fluxes, and hence of quality model input data, or of surface measurements.

References

Abbot, C. G. and Fowle, F. E.: Annals of the Astrophysical Observatory of the Smithsonian Institute, Smithsonian Institution, Vol. 2, 245 pp., 1908.

Arking, A., Chou, M.-D., and Ridgway, W. L.: On estimating the effects of clouds on atmospheric absorption based on flux observations above and below cloud level, Geophys. Res. Lett., 23, 829–832, 1996.

Briegleb, B. P., Minnis, P., Ramanathan, V., and Harrison, E.: Comparison of regional clear-sky albedos inferred from satellite observations and model computations, J. Clim. Appl. Meteor., 25, 214–226, 1986.

Budyko, M. I.: Heat balance of the earth's surface, U.S. Weather Bureau Memo. PB131692, 259 pp., 1956.

Budyko, M. I.: The Earth's Climate: Past and Future, Academic Press, 307 pp., 1982.

Cess, R. D., Dutton, E. G., DeLuisi, J. J., and Jiang, F.: Determining surface solar absorption from broadband satellite measurements for clear skies: Comparison with surface measurements, J. Climate, 4, 236–247, 1991.

Cess, R. D., Zhang, M. H., Minnis, P., et al.: Absorption of solar radiation by clouds: Observations versus models, Science, 267, 496-499, 1995.

Chen, C.-T. and Roeckner, E.: Validation of the Earth radiation budget as simulated by the Max Planck Institute for Meteorology general circulation model ECHAM4 using satellite observations of the Earth Radiation Budget Experiment, J. Geophys. Res., 101, 4269–4287, 1996.

Chen, J., Carlson, B. E., and Del Genio, A. D.: Evidence for strengthening of the tropical general circulation in the 1990s, Science, 295, 838–841, 2002.

Chou, M.-D., Arking, A., Otterman, J., and Ridgway, W. L.: The effect of clouds on atmospheric absorption of solar radiation, Geophys. Res. Lett., 22, 1885–1888, 1995.

Darnell, W. L., Staylor, W. F., Gupta, S. K., and Denn, F. M.: Estimation of surface insolation using Sun-synchronous satellite data, J. Climate, 1, 820–835, 1988.

Darnell, W. L., Staylor, W. F., Gupta, S. K., Ritchey, N. A., and Wilber, A. C.: Seasonal variation of surface radiation budget derived from International Satellite Cloud Climatology Project C1 data, J. Geophys. Res., 97, 15 741–15 760, 1992.

Del Genio, A. D., Yao, M.-S., Kovari, W., and Lo, K. K.-W.: A prognostic cloud water parameterization for global climate models, J. Climate, 9, 270–304, 1996.

Dickinson, R., Henderson-Sellers, R., and Kennedy, P.: Biosphere-Atmosphere Transfer Scheme (BATS) Version 1e as coupled to the NCAR Community Climate Model, Tech. Note NCAR/TN-387+STR, Natl. Cent. For Atmos. Res., Boulder, Colo., 1993.

Dines, W. H.: The heat balance of the atmosphere, Q. J. R. Meteorol. Soc., 43, 151–158, 1917.

Ebert, E. E. and Curry, J. A.: A parameterization of ice cloud optical properties for climate models, J. Geophys. Res., 97, 3831–3836, 1992.

Esbensen, S. K. and Kushnir, Y.: The heat budget of the global oceans: An atlas based on surface marine observations, Rep. 29, Clim. Res. Inst., Oreg. State Univ., Corvallis, 1981.

Ellis, J. S. and Vonder Haar, T. H.: Zonal average earth radiation budget measurements from satellites for climate studies, Atmos. Sci. Rep., 240, Colo. State Univ., Boulder, 1976.

Fotiadi, A., Hatzianastassiou, N., Matsoukas, C., Pavlakis, K. G., Drakakis, E., Hatzidimitriou, D., and Vardavas, I.: Analysis of the decrease in the tropical mean outgoing shortwave radiation at the top of atmosphere for the period 1984–2000, Atmos. Chem. Phys. Discuss., 5, 455–480, 2005,
SRef-ID: 1680-7375/acpd/2005-5-455.

Fowler, L. D. and Randal, D. A.: Liquid and ice cloud microphysics in the CSU general circulation model. Part II: Impact of cloudiness, the earth's radiation budget, and the general circulation of the atmosphere, J. Climate, 9, 530–560, 1996.

Garratt, J. R.: Incoming shortwave fluxes at the surface – A comparison of GCM results with observations, J. Climate, 7, 72–80, 1994.

Garratt, J. R., Prata, A. J., Rotstayn, L. D., McAvaney, B. J., and Cusack, S.: The surface radiation budget over oceans and continents, J. Climate, 11, 1951–1968, 1998.

Gautier, C., Diak, G., and Masse, S.: A simple physical model to estimate incident solar radiation at the surface from GOES satellite data, J. Appl. Meteorol., 19, 1005–1012, 1980.

Gilgen, H. and Ohmura, A.: The Global Energy Balance Archive, Bull. Am. Meteor. Soc., 80, 831–850, 1999.

Gilgen, H., Wild, M., and Ohmura, A.: Means and trends of shortwave irradiance at the surface estimated from Global Energy Balance Archive, J. Climate, 11, 2042–2061, 1998.

Gupta, S. K., Ritchey, N. A., Wilber, A. C., Whitlovk, C. H., Gibson, G. G., and Stackhouse Jr., P. W.: A climatology of surface radiation budget derived from satellite data, J. Climate, 12, 2691–2710, 1999.

Hartmann, D. L.: Aerosol-Cloud-Climate Interactions, Radiative effects of clouds on Earth's climate, International Geophysics Series, P. Hobbs, Acad. Press Inc., 54, 151–173, 1993.

Hartmann, D. L.: Global Physical Climatology, Academic Press, 411 pp., 1994.

Hatzianastassiou, N. and Vardavas, I.: Shortwave radiation budget of the Northern Hemisphere using International Satellite Cloud Climatology Project and NCEP/NCAR climatological data, J. Geophys. Res., 104, 24 401–24 421, 1999.

Hatzianastassiou, N. and Vardavas, I.: Shortwave radiation budget of the Southern Hemisphere using ISCCP C2 and NCEP/NCAR climatological data, J. Climate, 14, 4319–4329, 2001.

Hatzianastassiou, N., Fotiadi, A., Matsoukas, C., Drakakis, E., Pavlakis, K. G., Hatzidimitriou, D., and Vardavas, I.: Long-term global distribution of Earth's shortwave radiation budget at the top of atmosphere, Atmos. Chem. Phys., 4, 1217–1235, 2004a, SRef-ID: 1680-7324/acp/2004-4-1217.

5   Hatzianastassiou, N., Katsoulis, B., and Vardavas, I.: Global distribution of aerosol direct radiative forcing in the ultraviolet and visible arising under clear skies, Tellus, 56B, 51–71, 2004b.

Hatzidimitriou, D., Vardavas, I., Pavlakis, K., Hatzianastassiou, N., Matsoukas, C., and Drakakis, E.: On the decadal increase in the tropical mean outgoing longwave radiation for the period 1984–2000, Atmos. Chem. Phys., 4, 1419–1425, 2004,

10   SRef-ID: 1680-7324/acp/2004-4-1419.

Henderson-Sellers, A. and Wilson, M. F.: Surface albedo data for climate modelling, Rev. Geophys., 21, 1743–1778, 1983.

Henderson-Sellers, A. and Robinson, P. J.: Contemporary Climatology, John Wiley & Sons, 439 pp., 1986.

15   Hinkelman, L. M., Ackerman, T. P., and Marchand, R. T.: An evaluation of NCEP Eta model predictions of surface energy budget and cloud properties by comparison with measured ARM data, J. Geophys. Res., 104, 19 535–19 549, 1999.

Houghton, H. G.: On the annual mean balance of the Northern Hemisphere, J. Meteor., 11, 1–9, 1954.

20   Hoyt, D. V.: The radiation and energy budgets of the Earth using both ground-based and satellite-derived values of total cloud cover, NOAA Tech. Rep., ERL 362-ARL 4, 124 pp., 1976.

Intergovernmental Panel on Climate Change (IPCC): Climate Change 2001, The Scientific Basis, 881 pp., edited by: Houghton, J. T., Ding, Y., Griggs, D. J., et al., Cambridge Univ. Press,

25   New York, 2001.

Jacobowitz, H., Smith, N. L., Howell, H. B., Nagle, F. W., and Hickey, J. R.: The first 18 months of planetary radiation budget measurements from the Nimbus 6 ERB experiment, J. Atmos. Sci., 36, 502–507, 1979.

Kiehl, J. T. and Trenberth, K. E.: Earth's annual global mean energy budget, Bull. Am. Meteorol.

30   Soc., 78, 197–208, 1997.

Kiehl, J. T., Hack, J. J., Zhang, M. H., and Cess, R. D.: Sensitivity of a GCM climate to enhanced shortwave cloud absorption, J. Climate, 8, 2200–2212, 1995.

Kondratyev, K. Y.: Radiation Characteristics of the Atmosphere and the Earth's surface,

Earth's surface shortwave radiation budget

N. Hatzianastassiou et al.

Title Page

Abstract	Introduction
Conclusions	References
Tables	Figures

◀	▶
◀	▶
Back	Close

Full Screen / Esc

Print Version

Interactive Discussion

EGU

Amerind., SNew Delhi, 580 pp., 1973.

Koepke, P., Hess, M., Schult, I., and Shettle, E. P.: Global aerosol data set. Rep. No 243, Max-Planck Institut für Meteorologie, 44 pp., Hamburg, Germany, 1997.

Kuhn, M. H.: The role of land ice and snow in climate, in: Understanding Climate Change, Geophys. Monogr. Ser., edited by: Berger, A., Dickinson, R. E., and Kidson, J. W., American Geophysical Union, Washington, D.C., 52, 17–28, 1989.

Kyle, H. L., Mecherikunnel, A., Ardanuy, P., Lanning, P., Groveman, B., Garret-Gampbell, G., and Vonder Haar, T. H.: A comparison of two major earth radiation budget data sets, J. Geophys. Res., 95, 9951–9970, 1990.

Li, Z. and Leighton, H. G.: Global climatologies of solar radiation budgets at the surface and in the atmosphere from 5 years of ERBE data, J. Geophys. Res., 98, 4919–4930, 1993.

Li, Z., Leighton, H. G., Masuda, K., and Takashima, T.: Estimation of SW flux absorbed at the surface from TOA reflected flux, J. Climate, 6, 317–330, 1993.

Li, Z., Barker, H. W., and Moreau, L.: The variable effect of clouds on atmospheric absorption of solar radiation, Nature, 376, 486–490, 1995.

Li, Z., Moreau, L., and Arking, A.: On solar energy disposition: A perspective from observation and modelling, Bull. Am. Meteorol. Soc., 78, 53–70, 1997.

Liepert, B. G.: Observed reductions of surface solar radiation at sites in the United States and worldwide from 1961 to 1990, Geophys. Res. Lett., 29(12), doi:10.1029/2002GL014910, 2002.

Liou, K. N.: Radiation and cloud processes in the atmosphere. Theory, Observation and Modelling, Oxford University Press Inc., 487 pp., 1992.

Liou, K. N.: An introduction to atmospheric radiation, International Geophysics Series, Academic Press, 84, 583 pp., 2002.

London, J.: A study of the atmospheric heat balance, final report, contract AF 19(122)-165, Coll. Of Eng., N. Y. Univ., New York, 99 pp., 1957.

MacCracken, M. C.: Carbon dioxide and climatic change: Background and overview, Projecting the Climatic Effects of Increasing Carbon Dioxide, edited by: MacCracken, M. C. and Luther, F. M., U.S. Department of Energy, 1–23, 1985.

Manabe, S. and Strickler, R. F.: Thermal equilibrium of the atmosphere with a convective adjustment, J. Atmos. Sci., 21, 361–385, 1964.

National, Academy of Sciences: Understanding Climatic Change: A Program for Action, National Academy Press, 239 pp., 1975.

Earth's surface shortwave radiation budget

N. Hatzianastassiou et al.

Earth's surface shortwave radiation budget

N. Hatzianastassiou et al.

EGU

Ohmura, A. and Gilgen, H.: Re-evaluation of the global energy balance. Interactions between global climate subsystems: The legacy of Hann, Geophys. Monogr., International Union of Geodesy and Geophysics, 75, 93–110, 1993.

Ohmura, A., Gilgen, H., Hegner, H., Mueller, G., Wild, M., Dutton, E. G., Forgan, B., Froehlich, C., Philippona, R., Heimo, A., Koenig-Langlo, G., McArthur, B., Pinker, R., Whitlock, C. H., and Dehne, K.: Baseline Surface Radiation Network (BSRN/WCRP): New precision radiometry for climate research, Bull. Am. Meteorol. Soc., 79, 2115–2136, 1998.

Ohring, G. and Adler, S.: Some experiments with a zonally averaged climate model, J. Atmos. Sci., 35, 186–205, 1978.

Paltridge, G. W. and Platt, C. M. R.: Radiative Processes in Meteorology and Climatology, Elsevier, 318 pp., 1976.

Peixoto, J. P. and Oort, A. H.: Physics of Climate, Springer, N.Y., 520 pp., 1992.

Peng, L. I., Chou, M.-D., and Arking, A.: Climate studies with a multi-layer energy balance model. Part I: Model description and sensitivity to the solar constant, J. Atmos. Sci., 39, 2639–2656, 1982.

Pilewski, P. and Valero, F.: Direct observations of excess solar absorption by clouds, Science, 257, 1626–1629, 1995.

Pinker, R. T. and Laszlo, I.: Modelling surface solar irradiance for satellite applications on a global scale, J. Appl. Meteorol., 31, 194–211, 1992.

Ramanathan, V.: Scientific use of surface radiation budget for climate studies, Surface Radiation Budget for Climate Applications, NASA PR-1169, 58–86, 1986.

Ramanathan, V.: The role of Earth Radiation Budget studies in climate and general circulation research, J. Geophys. Res., 4075–4094, 1987.

Ramanathan, V., Subasilar, B., Zhang, G. J., Conant, W., Cess, R. D., Kiehl, J. T., Grassl, H., and Shi, L.: Warm pool heat budget and shortwave cloud forcing: S missing physics, Science, 267, 499–503, 1995.

Raschke, E., Vonder Haar, T. H., Bandeen, W. R., and Pasternak, M.: The annual radiation balance of the Earth-atmosphere system during 1967–70 from NIMBUS 3 measurements, J. Atmos. Sci., 30, 341–364, 1973.

Raschke, E., Gratzki, A., and Rieland, M.: Estimates of global radiation at the ground from the deduced data sets of the International Cloud Climatology Project, J. Climatol., 7, 205–213, 1987.

Roesch, A., Wild, M., Gilgen, H., and Ohmura, A.: A new snow cover fraction parameterization

for the ECHAM4 GCM, Clim. Dyn., 17, 933–946, 2001.

Roesch, A., Wild, M., Pinker, R., and Ohmura, A.: Comparison of surface spectral albedos and their impact on the general circulation model estimated surface climate, J. Geophys. Res., 107, D14, doi:10.1029/2001JD000809, ACL 13-1–ACL 13-8, 2002.

5 Rossow, W. B. and Lacis, A. A.: Global, seasonal cloud variations from satellite radiance measurements. Part II: Cloud properties and radiative effects, J. Climate, 3, 1204–1253, 1990.

Rossow, W. B. and Zhang, Y.-C.: Calculation of surface and top of atmosphere radiative fluxes from physical quantities based on ISCCP data sets 2. Validation and first results, J. Geophys. Res., 100, 1167–1197, 1995.

10 Rossow, W. B. and Schiffer, R. A.: Advances in understanding clouds from ISCCP, Bull. Am. Meteorol. Soc., 80, 2261–2287, 1999.

Rossow, W. B., Walker, A. W., Beuschel, D. E., and Roiter, M. D.: International Satellite Cloud Climatology Project (ISCCP). Documentation of new cloud datasets, Wold Meteorol. Org. Geneva, 115 pp., 1996.

15 Sasamori, T., London, J., and Hoyt, D. V.: Radiation budget of the Southern Hemisphere, Meteor. Monogr., 35, 9–23, 1972.

Schmetz, J.: Towards a surface radiation climatology: Retrieval of downward irradiance from satellites, Atmos. Res., 23, 287–321, 1989.

Schneider, S. H.: Climate Modeling, Sci. Amer., 256 (5), 72–80, 1987.

20 Sellers, P. J., Meeson, P. W., Hall, F. G., et al.: Remote sensing of the land surface for studies of global change: Models – algorithms – experiments, Remote. Sens. Environ., 51, 3–26, 1995.

Slingo, A.: A GCM parameterization for the shortwave radiative properties of water clouds, J. Atmos. Sci., 46, 1419–1427, 1989.

25 Stephens, G. L.: Optical properties of eight water cloud types, Tech. Pap. 36, CSIRO Div. of Atmos. Phys., 254 pp., 1979.

Stephens, G. L. and Greenwald, T. J.: The earth's radiation budget and its relation to atmospheric hydrology, 2, Observations of cloud effects, J. Geophys. Res., 96, 15 325–15 340, 1991.

30 Stephens, G. L., Campbell, G. G., and Vonder Haar, T. H.: Earth Radiation Budgets, J. Geophys. Res., 86, 9739–9760, 1981.

Stackhouse Jr., P. W., Cox, S. T., Gupta, S. K., Dipasquale, R. C., and Brown, D. R.: The WCRP/GEWEX Surface Radiation Budget Project Release 2: First results at 1 degree reso-

Earth's surface shortwave radiation budget

N. Hatzianastassiou et al.

EGU

lution. Preprints, 10th Conf. On Atmospheric Radiation: A Symp. With Tributes to the Works of Verner Suomi. Madison, WI, Am. Meteorol. Soc., 520–523, 1999.

Stanhill, G. and Cohen, S.: Global dimming: A review of the evidence for a widespread and significant reduction in global radiation with discussion of its probable causes and possible agricultural consequences, Agricult. Forest. Meteorol., 107, 255–278, 2001.

Suttles, J. T. and Ohring, G.: Surface radiation budget for climate applications, NASA Reference Publication 1169, NASA, Washington, DC, 132 pp., 1986.

Thekaekara, M. P. and Drummond, A. J.: Standard values for the solar constant and its spectral components, Nature Phys. Sci., 229, 6–9, 1971.

Torres, O., Barthia, P. K., Herman, J. R., Sinyuk, A., Ginoux, R., and Holben B.: A long-term record of aerosol optical depth from TOMS observations and comparison to AERONET measurements, J. Atmos. Sci., 59, 398–413, 2002.

Vardavas, I. and Carver, J. H.: Solar and terrestrial parameterizations for radiative convective models, Planet. Space Sci., 32, 1307–1325, 1984.

Vardavas, I. M. and Koutoulaki, K.: A model for the solar radiation budget of the Northern Hemisphere: Comparison with Earth Radiation Budget Experiment data, J. Geophys. Res., 100, 7303–7314, 1995.

Vonder Haar, T. H. and Suomi, V. E.: Measurements of the earth's radiation budget from satellites during a five-year period, J. Atmos. Sci., 28, 305–314, 1971.

Weare, B.-C.: Relationships between net radiation at the surface and the top of atmosphere derived from a general circulation model, J. Climate, 2, 193–197, 1989.

Wei, X., Hahmann, A. N., Dickinson, R. E., et al.: Comparison of albedos computed by land surface models and evaluation against remotely sensed data, J. Geophys. Res., 106, 20 687–20 702, 2001.

Whitlock, C. H., Charlock, T. P., Staylor, W. F., et al.: First global WCRP shortwave surface radiation budget dataset, Bull. Amer. Meteor. Soc., 76, 905–922, 1995.

Wielicki, B. A., Wong, T. M., Allan, R. P., et al.: Evidence for large decadal variability in the tropical mean radiative energy budget, Science, 295, 841–844, 2002.

Wild, M. and Ohmura, A.: The role of clouds and the cloud-free atmosphere in the problem of underestimated absorption of solar radiation in GCM atmospheres, Phys. Chem. Earth, 24B, 261–268, 1999.

Wild, M., Ohmura, A., Gilgen, H., and Roeckner, E.: Validation of general circulation model radiative fluxes using surface observations, J. Climate, 8, 1309–1324, 1995.

Earth's surface shortwave radiation budget

N. Hatzianastassiou et al.

EGU

Wild, M., Ohmura, A., Gilgen, H., Roeckner, E., Giorgetta, M., and Morcrette, J.-J.: The disposition of radiative energy in the global climate system: GCM-calculated versus observational estimates, Clim. Dyn., 14, 853–869, 1998a.

Wild, M., Ohmura, A., Gilgen, H., and Morcrette, J.-J.: The distribution of solar energy at the Earth's surface as calculated in the ECMWF Re-analysis, Geophys. Res. Lett., 25(23), 4373–4376, 1998b.

Wild, M., Ohmura, A., Gilgen, H., and Rosenfeld, D.: On the consistency of trends in radiation and temperature records and implications for the global hydrological cycle, Geophys. Res. Lett., 31, L11201, 2004.

Wittmeyer, I. L. and Vonder Haar, T. H.: Analysis of the global ISCCP TOVS water vapor climatology, J. Climate, 8, 325–333, 1994.

Yu, R., Zhang, M., and Cess, R. D.: Analysis of the atmospheric energy budet: A consistency study of available data sets, J. Geophys. Res., 108, 9655–9661, 1999.

Earth's surface shortwave radiation budget

N. Hatzianastassiou et al.

Title Page

Abstract	Introduction
Conclusions	References
Tables	Figures

│◄   ►│

◄   ►

Back   Close

Full Screen / Esc

Print Version

Interactive Discussion

EGU

Earth's surface shortwave radiation budget

N. Hatzianastassiou et al.

Table 1. Model computed mean annual hemispherical (NH is Northern Hemisphere, SH is Southern Hemisphere) and global averages of downward shortwave radiation (DSR) and net downward shortwave radiation (net DSR) at the Earth's surface for January, April, July, October, and the whole year, for the 17-year (1984–2000) period. The radiative fluxes are expressed in Wm^{-2}. Numbers in parenthesis are standard deviations and represent interannual variabilities of the means.

	NH	SH	Global
Downward Shortwave Radiation			
January	113.8(9.8)	234.8(20.7)	174.3(15.3)
April	209.8(16.5)	140.4(11.5)	175.1(14.0)
July	224.8(17.2)	105.6(7.7)	165.2(12.5)
October	148.6(12.0)	197.0(16.6)	172.8(14.3)
Annual	173.9(14.0)	169.3(14.3)	171.6(14.1)
Net Downward Shortwave Radiation			
January	98.6(2.7)	204.5(6.5)	151.6(4.6)
April	177.0(4.6)	127.5(3.4)	152.2(4.0)
Jul	193.6(5.1)	94.9(2.1)	144.2(3.6)
October	130.9(3.5)	171.6(4.3)	151.2(3.9)
Annual	149.6(3.9)	149.3(4.0)	149.4(4.0)

EGU

Table 2. Model mean annual hemispherical and global averages of downward shortwave radiation at the Earth's surface (DSR), and net downward shortwave radiation (i.e. absorbed) at the Earth's surface (Net DSR), as computed in this study, compared with values from others. NH is Northern Hemisphere, SH is Southern Hemisphere. The radiative fluxes are expressed in Wm^{-2}.

Study	DSR NH	DSR SH	DSR Globe	Net DSR NH	Net DSR SH	Net DSR Globe
Present Study (1984–2000)	173.9	169.3	171.6	149.6	149.3	149.4
Liou (2002)			189.0			161.0
Hatzianastassiou and Vardavas (2001)		174.0			160.0	
Hatzianastassiou and Vardavas (1999)	177.9			156.6		
Global Energy Balance Archive (GEBA)			169.0			151.0
Gupta et al. (1999) (8-yr 1983–1991)	186.7	182.6	184.7	160.2	161.5	160.9
CSU/GCM (Gupta et al., 1999)	202.3	200.5	201.4	177.4	178.9	178.2
NCAR/GCM2 (Gupta et al., 1999)				179.1	181.5	180.3
NCAR/GCM3 (Gupta et al., 1999)	194.4	194.4	194.4	169.0	173.4	171.2
Wild and Ohmura (1999 – ARPEGE)						174.0
Wild et al. (1999 – HadAM2b)						175.0
Wild (2004 – ECHAM5)			180.0			156.0
Wild et al. (1998a – ECHAM4)			170.0			147.0
Wild et al. (1998a – ECHAM3)			189.0			164.0
GCM studies (Wild et al., 1998a)						164.0–182.0
Garratt et al. (1998)			190.0–201			160.0–174.0
Kiehl and Trenberth (1997)						168.0
NASA/GEOS-1 (Li et al., 1997)						190.6
CCC/GCM2 (Li et al., 1997)						175.0
ERBE/Li (Li et al., 1997)						157.0
ISCCP/Rossow (Li et al., 1997)						165.0
ISCCP/Pinker (Li et al., 1997)						171.1
Del Genio et al. (1996)				172.0		
Fowler and Randall (1996)						172.0
Li et al. (1995)						157.0
Rossow and Zhang (1995)			193.4			165.1
Vardavas and Koutoulaki (1995)				156.5		
Hartmann (1994)						171.0
Li and Leighton (1993)				155.0	159.0	157.0
Ohmura and Gilgen (1993)						142.0

ACPD

5, 4545–4597, 2005

Earth's surface shortwave radiation budget

N. Hatzianastassiou et al.

Title Page

Abstract | Introduction

Conclusions | References

Tables | Figures

◄◄ | ►►

◄ | ►

Back | Close

Full Screen / Esc

Print Version

Interactive Discussion

EGU

Earth's surface shortwave radiation budget

N. Hatzianastassiou et al.

Table 2. Continued.

Study	DSR NH	DSR SH	DSR Globe	Net DSR NH	Net DSR SH	Net DSR Globe
Darnell et al. (1992)			173.0			151.0
Peixoto and Oort (1992)						171.0
Rossow and Lacis (1990)				169.0		
Rossow and Lacis (1990) GISS GCM				158.0		
Ramanathan (1987)						169.0
Schneider (1987)						154.0
Henderson-Sellers and Robinson (1986)						171.0
MacCracken (1985)						157.0
Budyko (1982)						157.0
Peng et al. (1982)				159.8		
Stephens et al. (1981)				177.2		
Ohring and Addler (1978)				177.9		
Hoyt (1976)				150.3		
Paltridge and Platt (1976)						174.0
National Academy of Sciences (1975)						174.0
Sasamori et al. (1972)		172.0		156.0		
Manabe and Strickler (1964)				165.0		
London (1957)				161.9		
NCEP Reanalysis (1982–1994)			207.0			162.0
ECMWF Reanalysis (1985–1993)			180.0			152.0
NASA Reanalysis (1981–1992)			219.0			191.0
NASA GEWEX Reanalysis (1983–1992)			186.2			164.6

EGU

Earth's surface shortwave radiation budget

N. Hatzianastassiou et al.

Table 3. Global and annual mean differences, Δ(DSR) and Δ(NDSR) in Wm^{-2}, in model computed downward SW radiation at the Earth's surface (DSR), and net downward SW radiation at the Earth's surface (Net DSR or NDSR), induced by variation (ΔV in relative percentage value, %) of the variable V (A_c, cloud cover; τ_c^s, cloud scattering optical depth; τ_c^a, cloud absorption optical depth; g_c, cloud asymmetry parameter; W_{H2O}, total precipitable water; W_{O3}, total ozone column abundance; W_{CO2}, total column carbon dioxide; R_g, surface albedo; ISR, incoming SW radiation at TOA; AOT, aerosol scattering optical depth; ϖ_{aer}, aerosol single scattering albedo; g_{aer}, aerosol asymmetry parameter). In parenthesis, is given the range of variation for Δ(DSR) and Δ(NDSR) at pixel (2.5-degree latitude-longitude) level, for each sensitivity test. Year 1988 is the reference case.

reference		174.01	151.76
V	ΔV	Δ(DSR)	Δ(NDSR)
Low-A_c	10	−3.20 (−22.05–0.12)	−2.79 (−21.06–0.03)
Middle-A_c	10	−2.24 (−17.51–0.39)	−1.87 (−16.46–0.12)
High-A_c	10	−2.05 (−15.30–0.85)	−1.83 (−14.6–0.8)
Low-τ_c^s	10	−1.17 (−5.92–0)	−1.04 (−5.64–0.1)
Middle-τ_c^s	10	−0.81 (−5.21–0)	−0.69 (−4.9–0.1)
High-τ_c^s	10	−1.07 (−5.84–0)	−0.96 (−5.53–0.02)
Low-τ_c^a	10	−0.32 (−1.64–0)	−0.30 (−1.56–0)
Middle-τ_c^a	10	−0.20 (−1.52–0)	−0.17 (−1.28–0)
High-τ_c^a	10	−0.25 (−1.37–0)	−0.22 (−1.11–0)
g_c	5	7.93 (0–20.64)	6.98 (−0.69–19.66)
W_{H2O}	10	−1.94 (−6.65–0.02)	−1.73 (−6.34–0.02)
W_{O3}	10	−0.72 (−3.37–0.01)	−0.61 (−1.55–0.01)
W_{CO2}	10	−0.1 (−0.51–0.01)	−0.08 (−0.33–0.01)
R_g	10	−1.05 (0.02–13.41)	−3.53 (−94.52–0)
ISR	1	1.74 (0–4.63)	1.52 (0–3.22)
AOT	10	−0.16 (−2.62–0.01)	−0.12 (−2.03–0.01)
ϖ_{aer}	10	0.58 (0–11.81)	0.44 (−0.01–8.0)
g_{aer}	10	0.26 (−0.02–4.79)	0.21 (−0.05–3.72)

EGU

Table 4. Baseline Surface Radiation Network (BSRN) stations with measurements of downward SW radiation (DSR) at surface in the period 1992-2000 used for validation of model DSR results. Lat is latitude; Lon is longitude; Elev is elevation (in m); Period is years for which each station gave quality checked DSR monthly fluxes; Bias is the average difference of computed and observed fluxes; RMS is the root mean square error of computed fluxes; Slope is the least-squares line slope and its uncertainty at the 95% confidence interval and N is number of mean monthly fluxes used.

Station Name	Lat	Lon	Elev.	Period	Bias	RMS	Slope	N
Ny Alesund, Norway	78.9	12.0	11	92–00	−13.85	24.45	0.92±0.09	37
Barrow, Alaska	71.3	−156.6	8	92–00	−14.56	34.42	0.85±0.08	72
Toravere, Estonia	58.4	26.8	70	99–00	3.39	7.47	0.98±0.06	11
Lindenberg, Germany	52.2	14.1	125	94–00	−17.27	22.71	0.86±0.03	74
Payerne, Switzerland	46.8	6.9	491	92–97	−2.44	11.30	0.97±0.04	50
Regina, Canada	50.2	−104.3	574	95–99	−19.85	24.21	1.02±0.05	57
Chesapeake Light, Virginia	36.9	−75.7	0	2000	−7.78	10.96	1.07±0.19	6
Carpentras, France	44.0	5.0	110	96–00	−9.95	11.83	0.99±0.02	44
Boulder, Colorado	40.0	−105.0	1577	92–00	−15.28	22.01	1.12±0.04	84
Tateno, Japan	36.0	140.1	25	97–00	−6.36	18.21	1.23±0.11	39
Bermuda	32.3	−64.8	8	92–00	5.03	16.02	1.05±0.05	104
Kwajalein, Marshal Islands	8.7	167.7	10	92–00	−6.75	12.02	0.83±0.07	104
Ilorin, Nigeria	8.5	4.6	350	92–95	29.10	36.11	1.34±0.35	26
Nauru Is.	−0.5	166.9	7	98–99	−11.74	14.01	0.89±0.33	8
Manus Is., Papua New Guinea	−2.1	147.4	6	2000	10.47	10.47	–	1
Alice Springs, Australia	−23.7	133.9	547	95–00	−15.86	17.61	0.97±0.03	70
Florianopolis, Brazil	−27.5	−48.5	11	94–99	2.24	13.00	0.67±0.33	14
De Aar, South Africa	−30.7	24.0	1311	2000	−14.52	18.04	0.86±0.16	6
Lauder, New Zealand	−45.0	169.7	370	99–00	−44.19	50.73	0.74±0.09	17
Georg von Neumayer, Antarctica	−70.6	−8.2	42	92–00	−45.79	58.00	0.67±0.06	31
Syowa, Antarctica	−69.0	39.6	29	94–00	−71.91	86.49	0.60±0.07	46
South Pole	−90.0	–	2841	92–00	−26.78	30.57	1.00±0.04	38

Title Page

Abstract | Introduction

Conclusions | References

Tables | Figures

◄◄ | ►►

◄ | ►

Back | Close

Full Screen / Esc

Print Version

Interactive Discussion

EGU

EGU
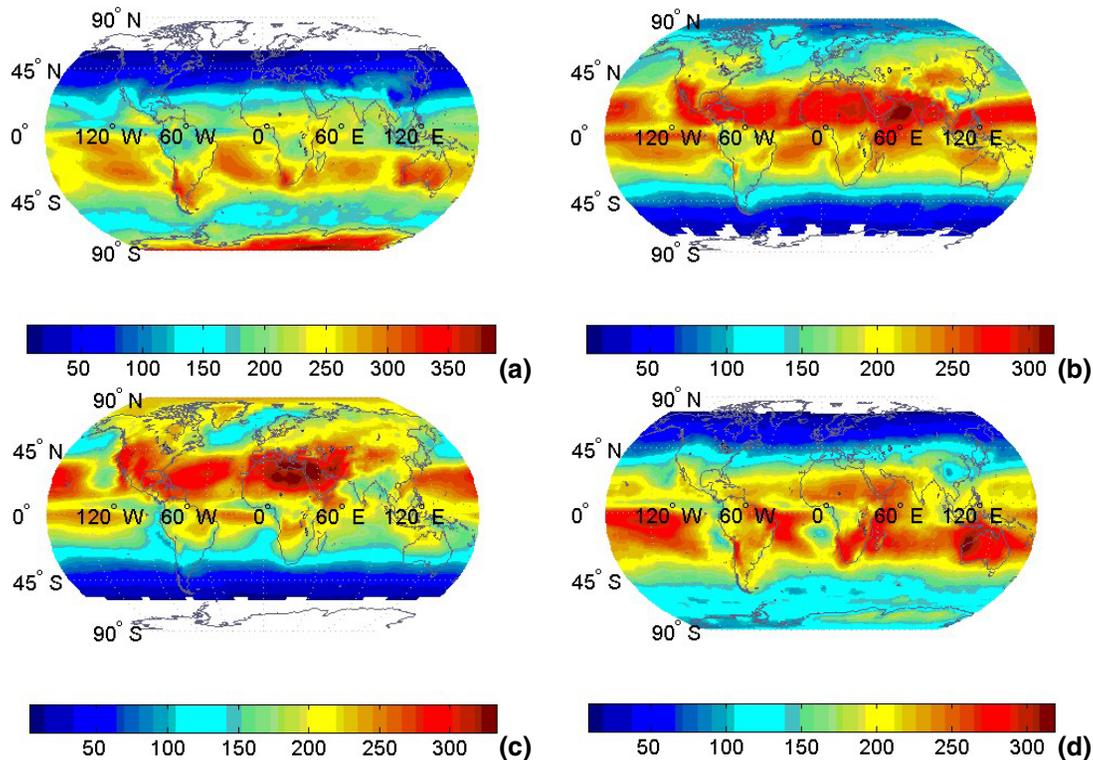
Fig. 1. Long-term (1984–2000) average global distribution of downward shortwave radiation (in Wm^{-2}) at the Earth's surface for the mid-seasonal months of **(a)** January, **(b)** April, **(c)** July, and **(d)** October.

EGU
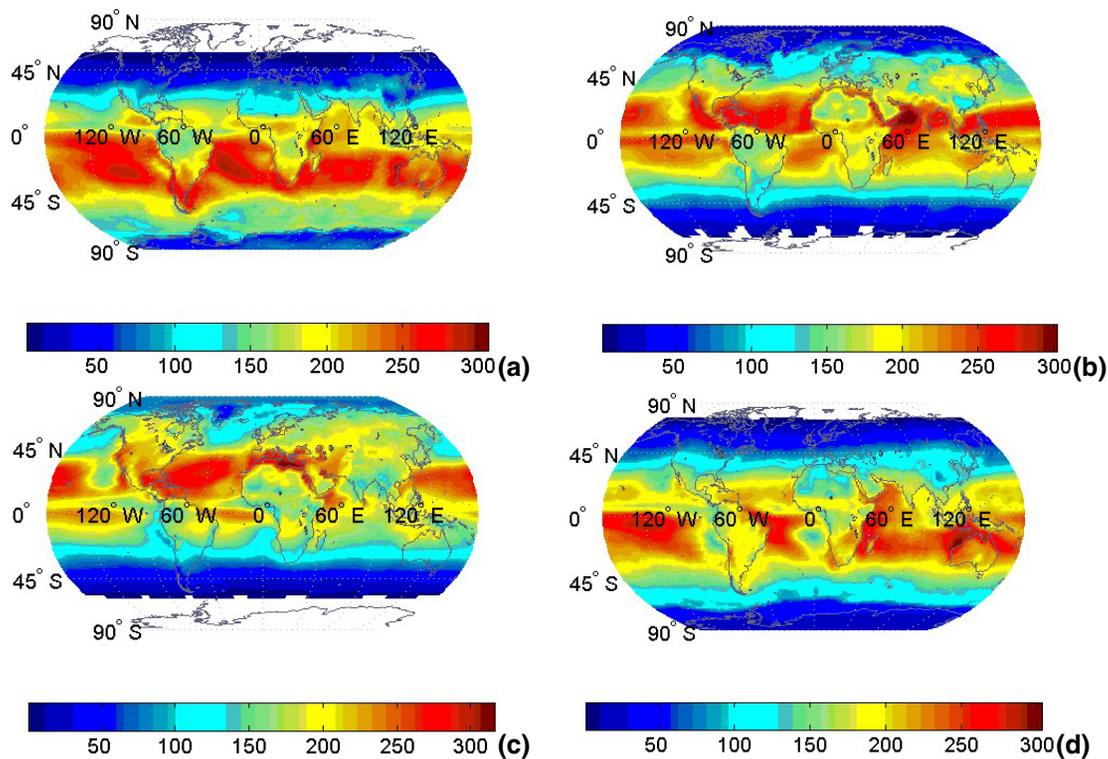
Fig. 2. Long-term (1984–1997) average global distribution of net downward (or absorbed) shortwave radiation (in Wm^{-2}) at the Earth's surface for the mid-seasonal months of **(a)** January, **(b)** April, **(c)** July, and **(d)** October.
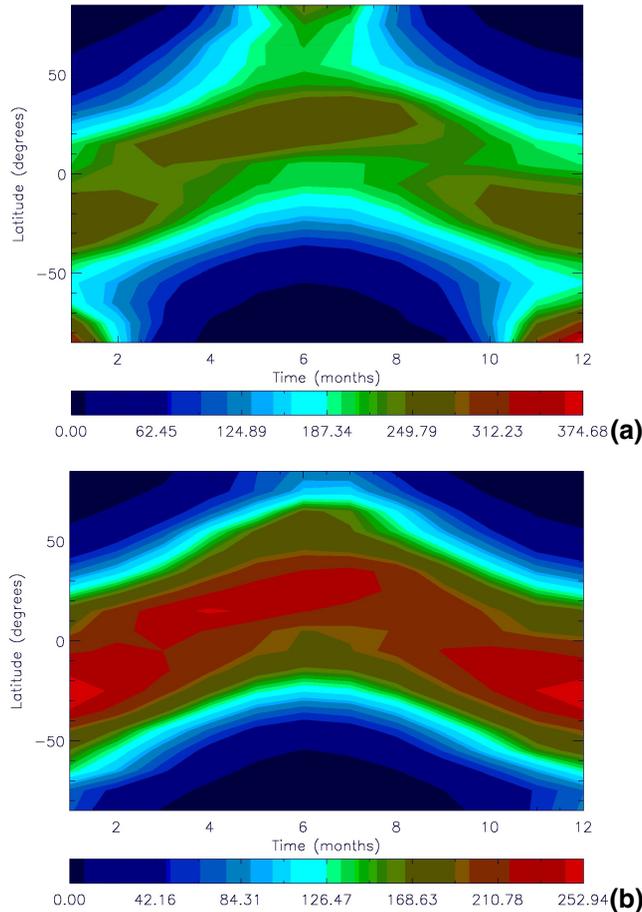
Fig. 3. Seasonal and latitudinal variation of 17-year (1984–2000) averages of monthly mean **(a)** downward shortwave radiation (DSR) at the Earth's surface and **(b)** net downward shortwave radiation (Net DSR) at the Earth's surface. Monthly mean quantities over a 2.5°×2.5° geographical grid are plotted.
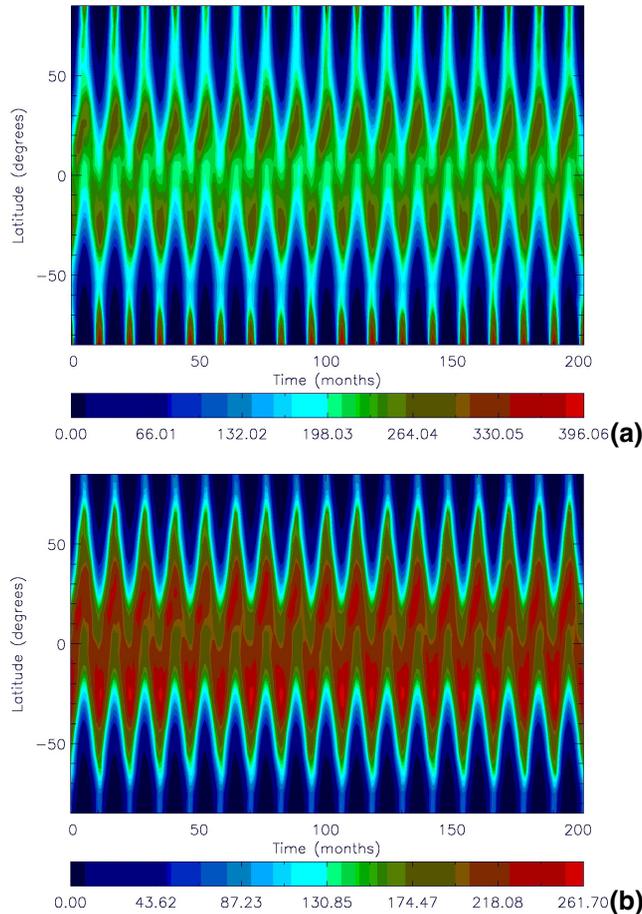
Fig. 4. Time-series of 10-degree latitude-zonal averages of monthly mean **(a)** downward shortwave radiation (DSR) at the Earth's surface and **(b)** net downward shortwave radiation (Net DSR) at the Earth's surface, for the period January 1984–December 2000. Monthly mean quantities over a 2.5°×2.5° geographical grid are used.
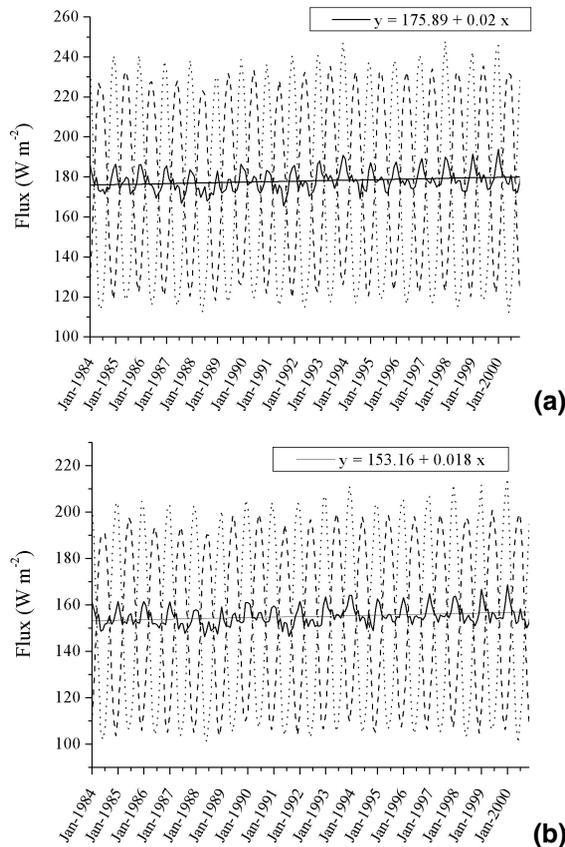
Fig. 5. Time series of monthly average: **(a)** downward shortwave radiation (DSR) at the Earth's surface (in Wm^{-2}) and **(b)** net downward (or absorbed) shortwave radiation (Net DSR) at the Earth's surface (in Wm^{-2}), for the 17-year (1984–2000) period for the Globe (solid lines), Northern Hemisphere (dashed lines), and Southern Hemisphere (dotted lines). The linear regression for the time series of the Globe is also shown.

Title Page

Abstract | Introduction

Conclusions | References

Tables | Figures

◄ | ►

◄ | ►

Back | Close

Full Screen / Esc

Print Version

Interactive Discussion

EGU
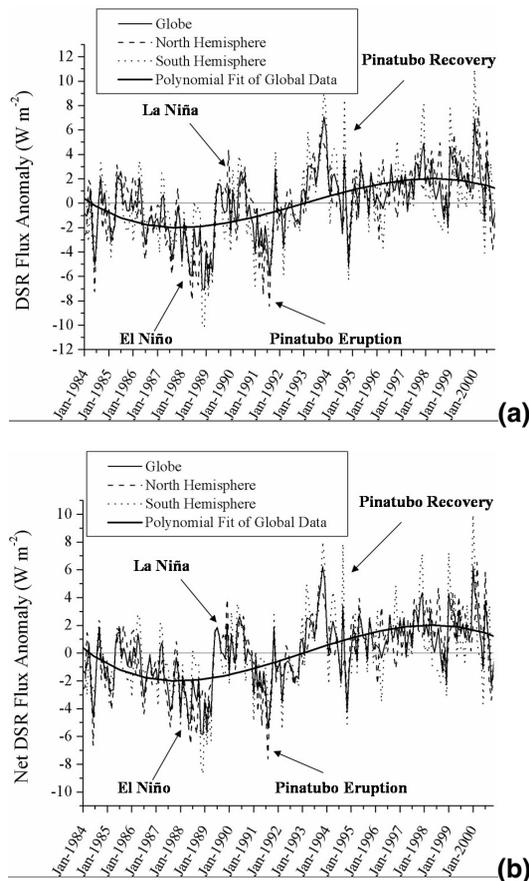
Fig. 6. Time-series of global and hemispherical averages of **(a)** downward shortwave radiation (DSR) flux anomalies (in Wm^{-2}) and **(b)** net downward shortwave radiation (DSR) flux anomalies (in Wm^{-2}) over the period 1984–2000 for the Globe (solid lines), Northern Hemisphere (dashed lines), and Southern Hemisphere (dotted lines). The 4th-order polynomial fit of the global data is also shown.

Title Page

Abstract | Introduction

Conclusions | References

Tables | Figures

◀ | ▶

◀ | ▶

Back | Close

Full Screen / Esc

Print Version

Interactive Discussion

EGU
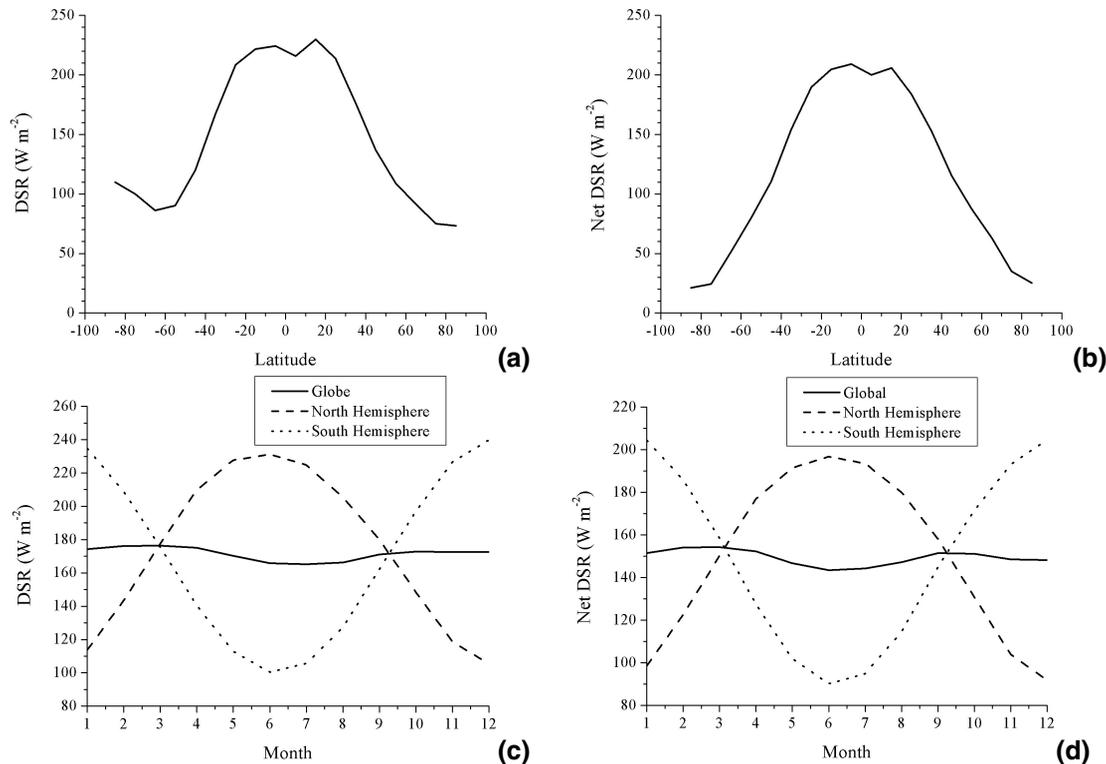
Fig. 7. Latitudinal variation of model computed: **(a)** mean annual downward shortwave radiation (DSR in Wm^{-2}) at the Earth's surface, and **(b)** mean annual net downward (or absorbed) shortwave radiation (Net DSR in Wm^{-2}) at the Earth's surface, for the period January 1984 through December 2000. Also shown is the seasonal variation of hemispherical and global averages of model computed: **(c)** downward shortwave radiation (DSR in Wm^{-2}) at the Earth's surface, and **(d)** net downward (or absorbed) shortwave radiation (Net DSR in Wm^{-2}) at the Earth's surface, for the period January 1984 through December 2000.

EGU

Title Page

Abstract | Introduction

Conclusions | References

Tables | Figures

|◄ | ►|

◄ | ►

Back | Close

Full Screen / Esc

Print Version

Interactive Discussion

EGU
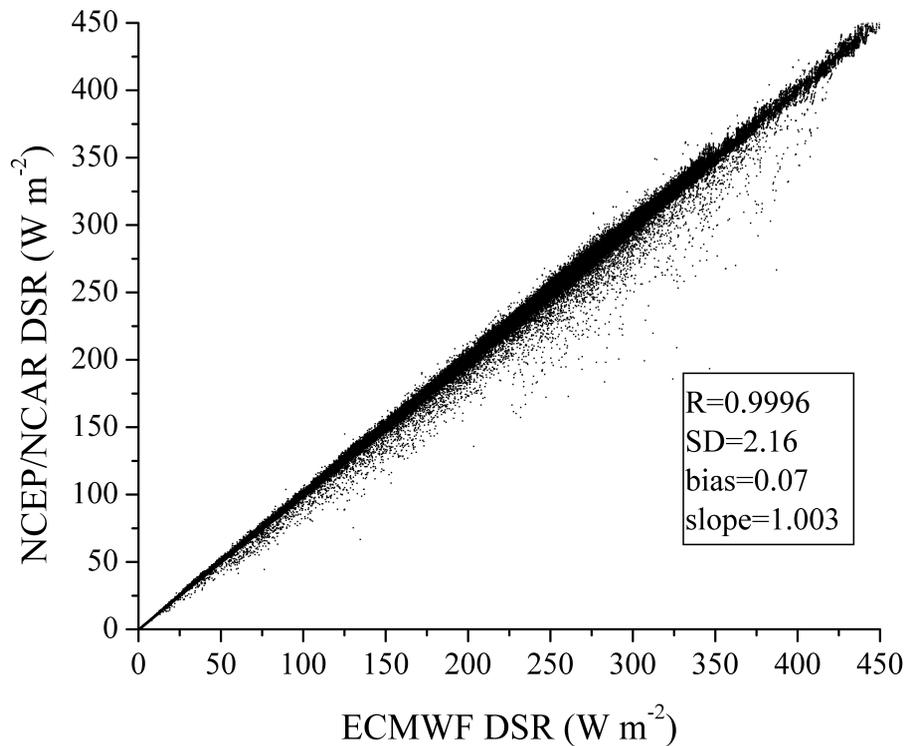
Fig. 8. Scatter plot comparison between model-computed downward shortwave radiation (DSR) at Earth's surface, over the time period 1986–1993, by using model input data for surface and atmospheric properties, taken from the NCEP/NCAR and ECMWF data bases.

Plot axis labels: NCEP/NCAR DSR (W m^{-2}) vs ECMWF DSR (W m^{-2})

Inset text: R=0.9996, SD=2.16, bias=0.07, slope=1.003
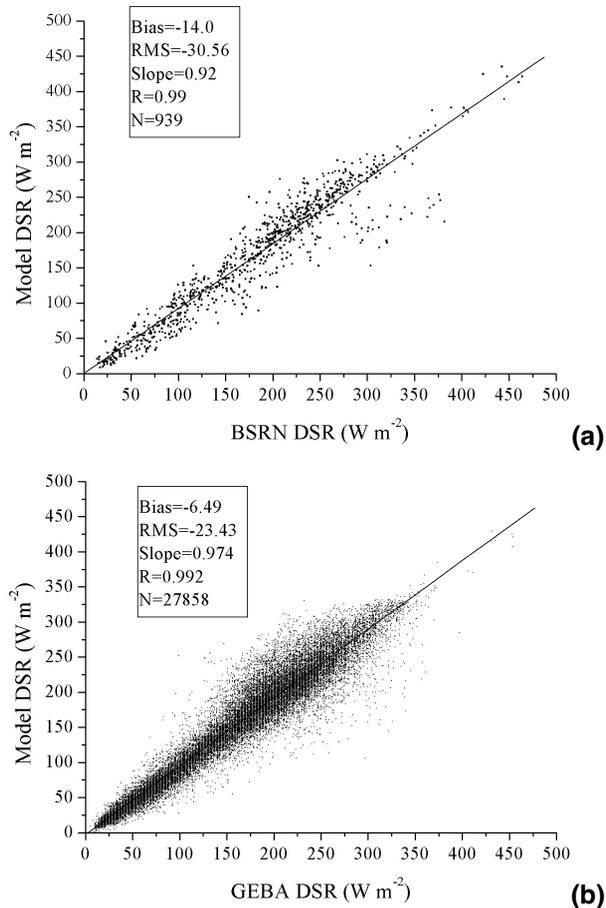
Fig. 9. Scatter plot comparison between model-computed and: **(a)** Baseline Surface Radiation Network (BSRN), and **(b)** Global Energy Balance Archive (GEBA) pixel data of monthly average downward shortwave radiation (DSR) at the Earth's surface, over the time periods 1992–2000 and 1984–2000, respectively.